
MoRe: Modular Representations for Principled Continual Representation Learning on Sequential Data

Jiaqi Sun^{1,2} Boyang Sun² Rasmy M. H.² Xiangchen Song¹ Kun Zhang^{1,2}
¹Carnegie Mellon University
²Mohamed bin Zayed University of Artificial Intelligence
{jiaqisun, kunz1}@cmu.edu

Abstract

Continual learning requires models to adapt to new data while preserving previously acquired knowledge. At its core, this challenge can be viewed as principled one-step adaptation: incorporating new information with minimal interference to existing representations. Most existing approaches address this challenge by modifying model parameters or architectures in a supervised, task-specific manner. However, the underlying issue is representational: tasks require distinct yet structured representations that can be selectively updated without disrupting representations, while structure should reflect intrinsic organization in the data rather than task boundaries. In sequential data, time-delayed dependencies provide a natural signal for uncovering this organization, revealing how fundamental representations give rise to more specific ones. Inspired by the modular organization of the human brain, we propose MoRe, a framework that identifies modularity in the representation itself rather than allocating it at the architectural level. MoRe decomposes knowledge into a hierarchy of fundamental and specific modules with identifiability guarantees, enabling principled module reuse, alignment, and expansion during adaptation while preserving old modules by construction. Experiments on synthetic benchmarks and real-world LLM activations demonstrate interpretable hierarchical structure, improved plasticity-stability trade-offs, suggesting MoRe as a principled foundation for continual adaptation.

1 Introduction

With the growing attention to foundation models, training such models in a sequential manner (driven by limited learning capacity and the inherently sequential flow of data) has brought the long-standing problem of Continual Learning (CL), or lifelong learning, back to the forefront. Generally speaking, the research problem of CL is how to avoid forgetting (or catastrophic forgetting) while acquiring new *abilities* during the learning procedure. In essence, without assuming that some part of the model remains stable, avoiding catastrophic forgetting is impossible.

Existing CL methods can be divided into supervised and unsupervised CL. Supervised CL directly models the *abilities* as tasks and aims to let the model conduct incremental tasks upon seeing more and more tasks, treating the data distribution as secondary. Representative methods constrain parameter updates, replay information from previous tasks, or isolate parameters across tasks; the architectural variants of the last category recognize that different tasks require different parts of the model, but how those parts are related is rarely addressed. Unsupervised CL, on the other hand, focuses on representation learning, yet most of its methods still operate via replay, distillation, regularization, or constraint modification. Across both settings, decisions about what to preserve and what to update are largely heuristic: there is no principled criterion, grounded in the structure of the data itself, for determining which parts of a representation should be reused and which should be replaced.

From this lens, the core of CL is representational: the specialization of model components determines what can be reused and what must be updated. We therefore tackle the problem of *continual representation learning*: how can a model form representations that grow cumulatively, across sequentially observed scenarios, without forgetting? This mirrors how cognition operates: understanding is updated continuously throughout life, and tasks are addressed by selecting the relevant pieces of understanding rather than by reshaping the system into a task-specific tool. Once rich representations are achieved, only a few samples are needed to assemble them for downstream tasks; the substantive challenge is the representation itself.

Inspired by the specialization and composition of modules in the human brain [29, 32], we propose Modular Representations (MoRe) for principled continual representation learning. The core idea is that representations should decompose into modules organized by a hierarchy from *fundamental* to *specific*, where fundamental modules are reused as building blocks for more specific ones. Crucially, this hierarchy should reflect intrinsic organization in the data rather than be imposed by task boundaries or architectural design.

Sequential data offers a particularly clear setting in which to identify such modular structure. Cross-layer time-delayed effects flow unidirectionally from fundamental to specific layers, providing the asymmetry needed to make the hierarchy identifiable up to within-layer indeterminacies and a compatible layer order. Identifiability is what turns modules from a useful inductive bias into well-defined objects: with identifiable modules, decisions about what to reuse and what to expand at each adaptation step become principled rather than heuristic, and the global representation can be recovered incrementally from a sequence of partial views.

Our contributions are as follows. (1) We propose Modular Representations (MoRe) for sequential data, decomposing the representation into a hierarchy that distinguishes fundamental from specific knowledge and reflects the data-generating process rather than task structure. (2) We provide identifiability guarantees for the modular hierarchy under cross-layer time-delayed dependencies, an estimation procedure for the initial dataset, and a one-step adaptation algorithm that selectively reuses, aligns, and expands modules under principled criteria. (3) On controlled synthetic benchmarks, we demonstrate factor recovery and plasticity-stability trade-offs. On real-world LLM activation data, we evaluate the emergence of hierarchical structure and the informativeness of the learned representations in one-step and continual learning settings.

2 Problem Setting

General Continual Representation Learning

We consider an underlying global distribution over time series, $\mathbf{X}_t \sim p(\mathbf{X}_t)$, with $\mathbf{X}_t \in \mathcal{X}$. For simplicity, we denote density functions by $p(\mathbf{X})$ when no particular values need to be involved. In practice, data are observed sequentially in batches, each a partial distribution of the global process: $\mathbf{X}_t^{(s)} \sim p_s(\mathbf{X}_t)$ with $\text{supp}(p_s) \subseteq \text{supp}(p)$. Each batch thus provides a limited temporal and statistical view of the underlying data-generating process. The goal is to learn an encoder $f : \mathcal{X} \rightarrow \mathcal{Z}$ such that $\mathbf{Z}_t = f(\mathbf{X}_t)$ exhibits desirable properties (disentanglement, reduced dimensionality, computational efficiency), incrementally from $\{\mathcal{D}_s \sim p_s\}_{s=1}^{\infty}$ rather than jointly from the full sequence. We refer to this paradigm as *General Continual Representation Learning*.

If f is naively updated on each batch, its effective domain and range may fail to cover \mathcal{X} or \mathcal{Z} , since each batch reveals only a partial view. Fundamentally, this limitation arises from the absence of explicit structure that would allow the domain and range of f to be extended incrementally and coherently across stages. To make such extension possible, the encoder must mirror structure that is already present in the data.

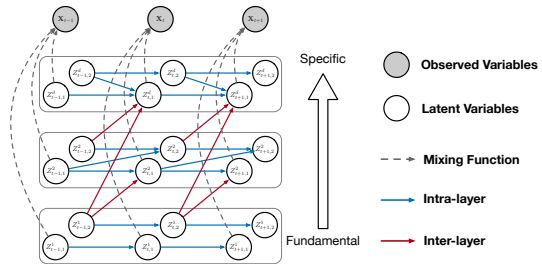


Figure 1: Sequential data with modular representations: higher layers are fundamental, lower layers specific; cross-layer time-delayed effects flow unidirectionally from fundamental to specific.

Data Generating Process with Modular Representations Real-world observations are typically generated by structured processes in which fundamental knowledge forms the basis for more specific knowledge—a pattern reflected, for example, in how cognition reuses general principles to construct domain-specific understanding. We adopt this view explicitly. The observation $\mathbf{X}_t \in \mathcal{X} \subset \mathbb{R}^n$ is generated from latent representations organized into d hierarchical layers $\mathbf{Z}_t^1, \dots, \mathbf{Z}_t^d$ with each $\mathbf{Z}_t^i \in \mathbb{R}^m$, via

$$\mathbf{X}_t = g(\mathbf{Z}_t), \quad \mathbf{Z}_t = \bigcup_{i=1}^d \mathbf{Z}_t^i, \quad (1)$$

where $g : \mathbb{R}^{m \times d} \rightarrow \mathbb{R}^n$ is a nonlinear mixing function, invertible on \mathcal{X} (hence $dm \leq n$). Higher layers encode fundamental, domain-agnostic knowledge (e.g., logic, physical principles); lower layers capture specialized, domain-specific information (e.g., finance, meteorology). Cross-layer dependencies are accordingly directed from higher to lower: abstract knowledge constrains specific representations, but not the reverse.

We further restrict cross-layer dependencies to be *time-delayed* rather than instantaneous, since hierarchical transformations across layers necessarily incur a non-zero temporal or computational delay; allowing instantaneous cross-layer interactions would violate this construction. Within-layer dependencies, generated at comparable levels of abstraction, are unrestricted. Each layer is therefore

$$\mathbf{Z}_t^i = f_i(\{\mathbf{Z}_{t-\tau}^i\}_{\tau=0}^L, \{\mathbf{Z}_{t-\tau}^j : 1 \leq j < i\}_{\tau=1}^L, \boldsymbol{\epsilon}_t^i), \quad (2)$$

with maximum lag L and mutually independent noise $\boldsymbol{\epsilon}_t^i$. We focus on lag-1 in the following. A critical consequence is that the layer assignment is not arbitrary: moving any latent variable to a different layer breaks the unidirectionality of cross-layer time-delayed effects. The hierarchy is anchored by the data itself, and this anchoring is what enables identifiability in Section 3.

From Modular Generative Process to Continual Learning This generative process gives the encoder f a structure to mirror: f decomposes into layer-wise modules that recover $\mathbf{Z}_t^1, \dots, \mathbf{Z}_t^d$ from \mathbf{X}_t . As we show in Section 3, the time-delayed unidirectional structure makes each layer’s representation identifiable up to within-layer indeterminacies and a compatible layer order: without which recovered components would be entangled functions of all latent factors, providing no handles for selective update. With identifiable modules, decisions about which to reuse, refine, or expand at each stage can be grounded in whether each module’s assumed structure is preserved on the new data, rather than chosen heuristically; fundamental modules naturally serve as reusable building blocks across stages. We make these claims precise in Section 3 and translate them into estimation and adaptation procedures in Section 4.

3 Theoretical Guarantees

Given the modular representations, we now establish identifiability of the learned representations when the data-generating process follows the assumed structure. This is crucial: only with identifiable representations can we develop principled learning algorithms and provide meaningful interpretations. Our identifiability result proceeds in three steps. First, Theorem 1 shows that instantaneous relations identify the latent variables up to within-layer transformations. Second, Theorem 2 shows that time-delayed effects identify the hierarchical order up to compatible permutations. Finally, Corollary 1 combines these results to establish identifiability of the full latent process. Note that all the proofs are given in single lag case, and the extension to multiple lags has been shown in [38, 14].

Theorem 1 (Identifiability of Latent Variables). *Suppose the observed sequential data \mathbf{X}_t follows the data generating process with modular representations. Suppose the following two conditions C1 and C2 hold, then any mixture among \mathbf{Z} can only happen within the same layer. Furthermore, when C3 holds, \mathbf{Z} are component-wise identifiability.*

C1 (Smooth and Positive Density). The conditional density $p(\mathbf{Z}_t | \mathbf{Z}_{t-1})$ is three times continuously differentiable and positive in \mathbf{R}^{md} .

C2 (Sufficient Variability). Let $\mathbf{W}_{t,i}^a \triangleq (\frac{\partial^2 \log p(\mathbf{Z}_t | \mathbf{Z}_{t-1})}{\partial Z_{t,i}^a \partial Z_{t-1,o}^{i'}})_{l' \in [d], o \in [m]}$, for $i \in [m], a \in [d]$, $\mathbf{U}_{t,i}^a \triangleq (\frac{\partial^3 \log p(\mathbf{Z}_t | \mathbf{Z}_{t-1})}{\partial Z_{t,i}^a \partial Z_{t-1,o}^{i'} \partial Z_{t-1,o}^{i'}})_{l' \in [d], o \in [m]}$ for $i \in [m], a \in [d]$, and $\mathbf{V}_{t,i,j}^a \triangleq$

$(\frac{\partial^3 \log p(\mathbf{Z}_t | \mathbf{Z}_{t-1})}{\partial Z_{t,i}^a \partial Z_{t,j}^a \partial Z_{t-1,o}^a})_{l' \in [d], o \in [m]}$ for $i < j \in [m], a \in [d]$. For each value of \mathbf{Z}_t , all functions $\mathbf{W}_{t,1}^1, \mathbf{U}_{t,1}^1, \mathbf{V}_{t,1,2}^1, \dots, \mathbf{W}_{t,m}^d, \mathbf{U}_{t,m}^d, \mathbf{V}_{t,m-1,m}^d$ are linearly independent.

C3 (Sparse Latent Process for Each Layer). For any $Z_{t,i}^a$, either its intimate neighbor set is empty, or it has a child with empty intimate neighbor set.

Proof Sketch The proof exploits the modular structure: instantaneous dependencies occur only within the same layer. Consequently, conditional on past latent variables, current latent variables from different layers are independent. This cross-layer conditional independence rules out mixing across layers, so any remaining mixing must occur within a layer. Under the sparsity condition C3, defined via the intimate neighbor set (Def. 1), existing within-layer results imply component-wise identifiability. Full proof is provided in Appendix A.2.

Having identified the latent variables up to layer-wise transformations, we next determine how the layers are ordered. The key observation is that time-delayed effects are directional and thus impose constraints on admissible layer permutations.

Theorem 2 (Identifiability of Hierarchical Order). *Suppose the observed sequential data \mathbf{X}_t follows the data-generating process with modular representations. Suppose the assumptions of Theorem 1 hold. Suppose further that:*

C4 (Hierarchical Mask Constraint). *The estimated transition model is constrained by a layer-wise hierarchical mask: under an estimated order $\hat{\pi}$, time-delayed effects from layer a to layer b are allowed only if $\hat{\pi}^{-1}(a) < \hat{\pi}^{-1}(b)$.*

C5 (Unique Compatible Order). *The true layer-level time-delayed graph admits a unique compatible order.*

Then any estimated hierarchical order that induces the same observational distribution as the true model must be compatible with the true layer-level time-delayed graph. In particular, the hierarchy is identifiable up to compatible order. Moreover, under C5, the hierarchical order is uniquely identifiable.

Proof Sketch By Theorem 1, cross-layer mixing is impossible, so the only remaining ambiguity is a permutation of layers. A compatible order is one that does not reverse any true time-delayed effect. Suppose an estimated order violates this constraint. Then a true effect from layer a to layer b would be disallowed by the mask in C4, so the estimated model could not reproduce the true transition distribution. This contradicts distributional equivalence. Therefore, only compatible orders are admissible. If C5 holds, the compatible order is unique, yielding identifiability.

We now combine the two results to characterize identifiability of the entire latent process.

Corollary 1 (Identifiability of the Latent Process). *Suppose the observed sequential data \mathbf{X}_t follows the data-generating process with modular representations. Suppose the assumptions of Theorem 1 and Theorem 2 hold. Suppose further that the latent variables are within-layer component-wise identifiable, for example by [14]. Then the full latent process is identifiable up to compatible hierarchical order. If C5 holds, then the full latent process is identifiable up to the remaining component-wise indeterminacies.*

Proof Sketch Theorem 1 identifies the layer partition by ruling out cross-layer mixing. Within each layer, component-wise identifiability resolves the remaining ambiguity. Theorem 2 then restricts the admissible layer permutations to compatible orders determined by time-delayed effects. Therefore, the full latent process is identifiable up to compatible order. If C5 holds, the order is unique, and the entire process is identifiable up to standard component-wise indeterminacies.

Remark The focus of the work is to recovering the hierarchical structure, i.e., cross-layer relations, and the identifiability of the components free from the permutation cross layers. Therefore, in the following sections, instantaneous relations will not be included, in order to make it a more concentrated study, and [14] has provided a comprehensive study.

Given the identifiability of the hierarchical modular representation, we now design an estimation procedure to recover these representations, and an adaptation procedure that preserves previously learned components while recovering new components from incoming data.

4 Method

We propose **MoRe** (Modular Representation Learning), a framework for unsupervised continual representation learning from sequential data. MoRe learns hierarchical modular representations on an initial dataset and adapts them across subsequent datasets by selectively reusing previously learned modules, aligning shared representations, and expanding only when new modules are needed.

4.1 Learning Modular Representations on the Initial Dataset

We first estimate the modular representation from the initial dataset \mathcal{D}_0 . The objective is to learn an encoder f that maps observations \mathbf{X}_t to hierarchical modular representations \mathbf{Z}_t , exploiting the asymmetry established by Theorems 1–2: cross-layer time-delayed effects are unidirectional from fundamental to specific layers.

Coordinate Projection The observation $\mathbf{X}_t \in \mathbb{R}^n$ typically lies near a lower-dimensional subspace, and the latent representation has total dimension $md \leq n$ by construction. We therefore fit a coordinate basis $\mathbf{V}_0 \in \mathbb{R}^{n \times d_0}$ from the principal directions of \mathcal{D}_0 , with mean $\boldsymbol{\mu}_0$, and project the data: $\mathbf{X}_t^{\text{proj}} = (\mathbf{X}_t - \boldsymbol{\mu}_0)\mathbf{V}_0$. This removes redundant observation dimensions before encoding and establishes a shared coordinate system in which subsequent datasets can be expressed (Section 4.2), making module reuse well-defined under shifting input distributions. The encoder f is learned on $\mathbf{X}_t^{\text{proj}}$.

Joint Estimation When model capacity permits, we estimate all layers simultaneously by maximizing the conditional likelihood $p(\mathbf{X}_t^{\text{proj}} | \mathbf{X}_{t-1}^{\text{proj}})$ subject to a layer-wise structural constraint on the latent transitions. By the change-of-variables formula, this yields the objective

$$\mathcal{L}_{\text{joint}} = \mathbb{E}_{\mathbf{X}_t^{\text{proj}}, \mathbf{X}_{t-1}^{\text{proj}}} [-\log p(\mathbf{Z}_t | \mathbf{Z}_{t-1})] + \log |\det \mathbf{J}_{f^{-1}}| + \gamma \|\mathbf{J}_B\|_1, \quad (3)$$

where $\mathbf{J}_B = \partial \mathbf{Z}_t / \partial \mathbf{Z}_{t-1}$ is the time-delayed transition Jacobian, constrained to be block lower-triangular according to the layer order, and γ controls the sparsity of cross-layer dependencies. Prior work on temporal latent identification provides both nonparametric and parametric instantiations [38, 14, 28].

Layer-wise Estimation When joint estimation is computationally infeasible, MoRe estimates the hierarchy progressively: fundamental layers are recovered first from the marginal temporal structure, and higher layers are then estimated conditional on the learned lower-level modules. This variant mirrors the developmental acquisition of structured representations; full details and empirical evaluation are in Appendix B.1.

4.2 Principled Continual Adaptation

Given a new dataset \mathcal{D}_k and the previously learned encoder f_{k-1} , basis \mathbf{V}_{k-1} , and transition $\mathbf{J}_B^{(k-1)}$, adaptation proceeds in two phases: an inference-only *fitting and assessment* phase that uses existing structure to comprehend new data and identify what is missing, followed by a *selective updating* phase that aligns reused modules, introduces new ones where needed, and select a sparse set.

Fitting and Assessment Just as one first interprets new observations through current understanding before revising belief, MoRe begins by applying f_{k-1} to \mathcal{D}_k without any training. The new data are projected into the existing coordinate system, $\mathbf{X}_k^{\text{proj}} = (\mathbf{X}_k - \boldsymbol{\mu}_{k-1})\mathbf{V}_{k-1}$, and passed through the existing modules to obtain candidate latents and transition residuals. Two diagnostics are then computed. First, for each existing module j , a static *self-consistency score* $a_j \in [0, 1]$ measures whether j 's assumed generative structure is preserved on \mathcal{D}_k — specifically, whether j remains temporally autocorrelated and whether its past leaks into other modules' residuals (cf. the cross-layer conditional independence underlying Theorem 1). Modules whose structure is preserved score

high; modules that no longer fit score low. Second, the reconstruction residual in observation space, $\mathbf{R} = \mathbf{X}_k - (\mathbf{X}^{\text{proj}} \mathbf{V}_{k-1}^\top + \boldsymbol{\mu}_{k-1})$, is analyzed via its principal directions, yielding candidate new coordinates \mathbf{V}^{new} orthogonal to \mathbf{V}_{k-1} and a corresponding allocation of candidate new modules. The transition is extended to a layer-respecting block structure $\mathbf{J}_B^{\text{ext}}$, allowing time-delayed effects from existing to candidate new modules but forbidding the reverse. Detailed forms of a_j and the residual analysis are deferred to Appendix C.

Selective Updating Adaptation then commits to which modules to retain and how to refine them. Each module is associated with a Hard Concrete gate [17] $g_j \in [0, 1]$, since module selection consists of independent binary decisions rather than a categorical choice. The self-consistency score a_j informs only the gate *prior* (its initialization), not a runtime suppressor: existing modules with high a_j start with positive logits, those with low a_j start negative, and the magnitude of this initialization is itself attenuated when no module is clearly self-consistent, leaving selection to the data (details in Appendix C.3). Reused modules are also passed through a learnable alignment T , initialized to identity, which permits small coordinate adjustment while keeping it close to identity. The adapted representation is

$$\mathbf{Z}_t = T\left(f_{k-1}(\mathbf{X}_t^{\text{proj}})\right) \odot \mathbf{g}^{\text{old}} \oplus f^{\text{new}}\left((\mathbf{X}_k - \boldsymbol{\mu}_{k-1})\mathbf{V}^{\text{new}}\right)_t \odot \mathbf{g}^{\text{new}}, \quad (4)$$

with residual $\mathbf{E}_t = \mathbf{Z}_t - \mathbf{J}_B^{\text{ext}}(\mathbf{Z}_{t-1})$. The trainable components are T , the new encoder f^{new} , the new blocks of $\mathbf{J}_B^{\text{ext}}$, and the gate logits; f_{k-1} and the existing block of \mathbf{J}_B remain frozen. The objective combines a data fit term, an alignment regularizer, sparsity on gates, and sparsity on the new transition blocks:

$$\mathcal{L}_{\text{adapt}} = \mathcal{L}_{\text{data}}(\mathbf{E}_t, f^{\text{active}}) + \lambda_{\text{align}} \mathcal{R}(T) + \lambda_{\text{sp}}^{\text{old}} \mathcal{L}_0(\mathbf{g}^{\text{old}}) + \lambda_{\text{sp}}^{\text{new}} \mathcal{L}_0(\mathbf{g}^{\text{new}}) + \lambda_J \|\mathbf{J}_B^{\text{new}}\|_1. \quad (5)$$

Here $\mathcal{L}_{\text{data}}$ is the change-of-variables likelihood under the modular generative process, restricted to active modules; $\mathcal{R}(T)$ keeps T close to identity, which provides a continuous interpolation between full reuse and partial modification rather than a discrete reuse/modify dichotomy; \mathcal{L}_0 is the expected number of active gates under the Hard Concrete relaxation; and $\|\mathbf{J}_B^{\text{new}}\|_1$ encourages parsimonious new dependencies. Module selection is committed at the end of training by binarizing the gates: existing modules with $g_j^{\text{old}} = 0$ are deactivated for \mathcal{D}_k but retained in the library, and candidate new modules with $g_j^{\text{new}} = 1$ are added. The full algorithm is given in Appendix C.5.

Overview of MoRe MoRe addresses continual representation learning through two coupled mechanisms: a hierarchical modular representation, identifiable via the unidirectional cross-layer time-delayed structure of sequential data, and a two-phase adaptation procedure that turns identifiability into actionable updates. The first phase interprets new data with existing modules without training, scoring each module for self-consistency and surfacing missing structure as candidate directions; the second phase selectively aligns, retains, or expands modules through learnable gates whose prior is shaped by the self-consistency scores. The result is an adaptation step that reuses fundamental structure by default, and only modifies or expands modules when the data require it, to preserve prior knowledge while incrementally extending the global module library.

5 Experiments

Our experiments are organized to verify MoRe both as a principled mechanism and as a practically useful representation learner. Controlled synthetic experiments isolate the questions of identifiability, plasticity-stability, and selective module allocation under known ground truth, while real-world LLM activation experiments examine whether the learned hierarchical structure emerges in natural data and translates into label-efficient downstream prediction.

5.1 Synthetic Experiments

We separate scale from mechanism. Large-scale synthetic experiments test identifiability and structural recovery, while low-dimensional controlled systems allow exact analysis of adaptation, forgetting, and module selection.

Setup. We generate sequential latent data following the modular generative process of Equations (1) and (2), with both linear ($md \in \{4, \dots, 128\}$) and nonlinear ($md \in \{4, \dots, 16\}$) mixing across depths $L \in \{2, 3, 4\}$. For S-RQ1 we sweep latent dimensionalities and depths to test identifiability at scale; for S-RQ2 and S-RQ3 we focus on a controlled linear setting with seven transition scenarios spanning no shift, shared-factor shifts, missing or newly introduced specific factors, irrelevant-old-module presence, and multi-stage sequences (full specifications in Appendix E.2). We measure latent recovery via the Mean Correlation Coefficient (MCC), forgetting by the drop in old-factor MCC after adaptation, and gate accuracy by whether reused and expanded modules are correctly assigned. We compare against fine-tuning, reuse-only, and ablations of MoRe’s alignment matrix T and sparsity penalties.

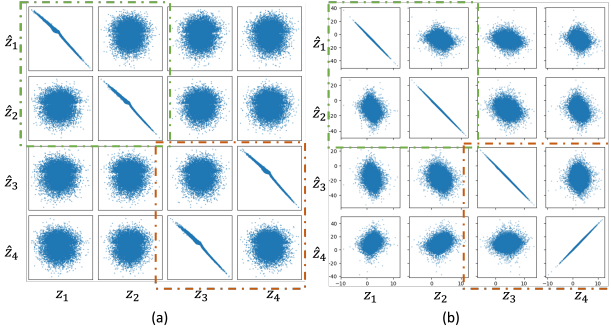


Figure 2: The scatter plot of estimated latents with true for (a) nonlinear case, and (b) linear case.

Type	Dimensions of layers	MCC
Linear	[2, 2]	0.99
	[4, 4]	0.99
	[8, 8, 8]	0.99
	[16, 16, 16, 16]	0.93
	[32, 32, 32, 32]	0.85
Nonlinear	[2, 2]	0.98
	[4, 4]	0.98
	[8, 8]	0.98
	[3, 3, 3]	0.97
	[4, 4, 4, 4]	0.96

Table 1: Comparison of MCC for Linear and Nonlinear Models

S-RQ1: Can MoRe identify hierarchical components? In this section, we empirically evaluate our proposed framework using synthetic time series data generated through fixed causal processes as illustrated in Equation (2), (1) and Figure 1. To validate our theoretical results across varying complexities, we investigate linear generation with overall latent dimensions $md \in \{4, \dots, 128\}$ and nonlinear generation with $md \in \{4, \dots, 16\}$ across depths of $L \in \{2, 3, 4\}$.

Quantitatively, we employ the Mean Correlation Coefficient (MCC) to measure the alignment between ground-truth and recovered latents. As shown in Table 1, our method achieves satisfying performance across both regimes, consistently recovering the latent space even as dimensionality increases. These results empirically confirm the identifiability of our model and validate the strength of our theoretical guarantees.

Qualitatively, Figure 2 displays the scatter plots between ground-truth latents z and estimated latents \hat{z} for the 2-layer, 4-variable case in both linear (a) and nonlinear (b) regimes. The emergence of clear diagonal alignments confirms high-fidelity recovery of the latent components. Notably, as highlighted by the dashed blocks, our modular-level estimation constrains the permutation indeterminacy. While traditional methods may permute variables globally, our results demonstrate that permutations occur only within their respective layers (e.g., z_1, z_2 and z_3, z_4 are grouped), thereby preserving the block-causal structure and validating our theoretical framework for structured identifiability.

S-RQ2: Does MoRe adapt correctly without forgetting? Figure 3a reports plasticity (target MCC) and stability (forgetting) across six transition scenarios. MoRe matches or exceeds fine-tuning plasticity on scenarios requiring no expansion (C1, C6) while achieving near-zero or negative forgetting—meaning adaptation actively improves old-factor recovery. On expansion scenarios (C2–C5), fine-tuning recovers new factors well but at the cost of catastrophic forgetting (up to +0.19 on C4), whereas MoRe maintains stability by isolating adaptation to new modules. Removing the alignment matrix (MoRe w/o T) preserves plasticity but consistently raises forgetting by ~ 0.15 across all cases, confirming that T is the primary mechanism protecting old representations during adaptation. Since scratch discards the old encoder entirely (forgetting undefined) and expansion only freezes it (forgetting zero by construction), neither is included in the stability comparison.

S-RQ3: Does selective adaptation enable correct factor allocation? Figure 3b evaluates gate decision accuracy: whether reused modules correctly avoid absorbing new factors and new modules

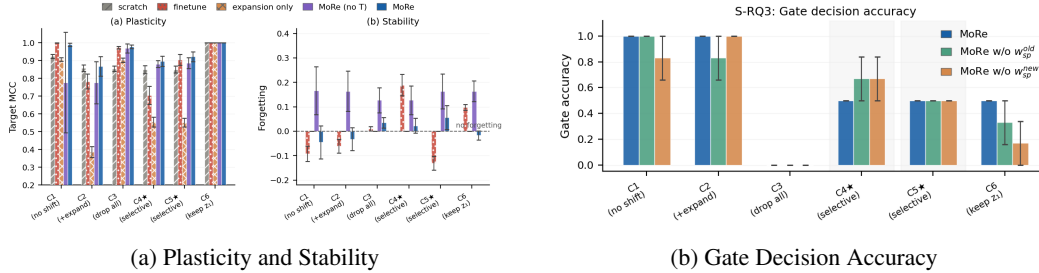


Figure 3: Plasticity, stability compared with baselines and gate decision accuracy

are correctly activated. On simple transitions (C1, C2, C6) MoRe achieves perfect gate accuracy, correctly routing factors without parameter growth in the old subspace. On the hard selective cases (C4*, C5*), accuracy drops to 0.5, reflecting inherent ambiguity when old and new factors partially overlap; both sparsity penalties (w_{sp}^{old} , w_{sp}^{new}) are required—removing either one further degrades gate decisions, confirming that correct factor allocation depends on explicit regularization of both module types.

5.2 Real-world LLM Activation Experiments

We evaluate whether the modular and hierarchical structure learned by MoRe emerges in real-world data (RW-RQ1) and whether it improves downstream prediction (RW-RQ2). LLM activations are a natural test case: they encode rich semantic information that is potentially organized hierarchically.

Setup. We include three datasets for evaluation in this section, namely: Arxiv*, AMPS[†], and Wikipedia[‡]. The reason for choosing these three datasets is they have reference in the data for locating the hierarchical structure (we manually set the hierarchy to 4 in the real-world experiments). For arXiv, we use the metadata subject category (e.g. math.LO, q-bio.PE) directly as the hierarchy label; for AMPS, we assign difficulty tiers via keyword matching against problem text (e.g. *add/multiply* → tier 0, *eigenvalue/determinant* → tier 3); and for Wikipedia, we proxy specificity by article word count, with short stubs treated as general and long articles as specific. To extract the activations from them, we use open-source LLMs including Pythia-1.4b [3] and Gemma-2-9b [31]. More details of LLM activation data processing are included in the Appendix E.2.

RW-RQ1: Does MoRe uncover broad-to-specific structure in real-world data? We evaluate alignment between MoRe’s learned hierarchy and externally defined abstraction levels, measuring *concept concentration* per layer and *cross-layer temporal dependencies* via the B -matrices. For each datasets, we trained 3 models to get meaningful results.

Concept concentration. For each MoRe layer we compute a concentration coefficient measuring how selectively a concept fires within one difficulty tier versus uniformly across all tiers. On AMPS, whose labels encode an explicit mathematical curriculum, concentration decreases monotonically from $\mu=0.054$ at L0 to $\mu=0.039$ at L3 (Figure 4), with L0 consistently above the null control ($\mu\approx 0.040$, shuffled labels). As shown in Table 2, the L0>L1 ordering holds across *all* 18 settings and datasets, while the mean L0–L2 gap is substantially larger on AMPS than on arXiv and Wikipedia, confirming that cleaner label hierarchies yield stronger alignment from MoRe.

Table 2: MoRe recovered hierarchy consistency with defined labels

Dataset	L0>L1	L1>L2	L2>L3	Mean L0–L2	Mean L0–L3
AMPS	6/6	5/6	2/6	0.0175 ± 0.004	0.0147 ± 0.002
Wikipedia	6/6	5/6	1/6	0.0045 ± 0.002	0.0035 ± 0.002
arXiv	6/6	2/6	0/6	0.0039 ± 0.005	-0.005 ± 0.007

*<https://www.kaggle.com/datasets/Cornell-University/arxiv>

†<https://huggingface.co/datasets/sarahpann/AMPS>

‡<https://huggingface.co/datasets/wikimedia/wikipedia>

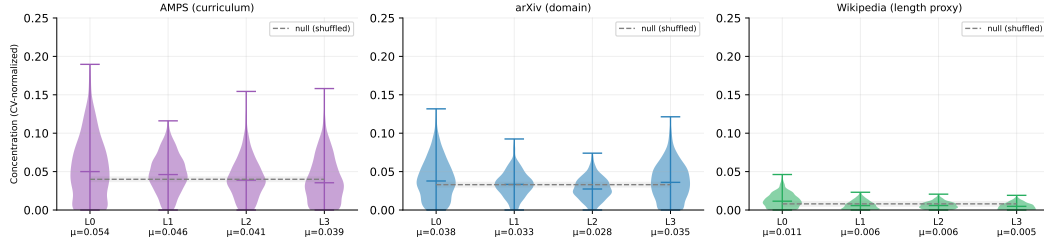


Figure 4: Per-layer concept concentration across three datasets

Table 3: Linear probe accuracy on AMPS tier prediction (MoRe).

Repr.	Dim	$n=10$	$n=25$	$n=50$	$n=100$	$n=1000$
PCA	256	77.0±2.9	83.0±2.1	84.6±1.5	84.8±0.8	84.9±0.6
MoRe_all	256	79.3±4.0	83.1±1.1	84.3±1.1	84.1±0.8	85.4±0.3
MoRe_L0	64	79.0±4.0	82.5±0.9	84.2±1.7	84.5±0.4	86.0±0.3
MoRe_L1	64	79.4±3.6	82.8±1.0	84.4±0.9	84.4±0.8	86.0±0.5
MoRe_L2	64	80.0±4.1	83.0±1.1	84.5±0.8	84.6±1.3	85.7±0.3
MoRe_L3	64	79.3±3.6	82.4±1.2	83.1±1.6	83.8±0.8	86.1±0.4

Cross-layer B-link chains. In the Appendix E.4.1, we trace the labels connected by cross-layer B -matrix links and show curriculum-consistent transitions on AMPS and abstract subfields to applied domains transitions from Arxiv.

RW-RQ2: Do MoRe representations improve label-efficient downstream prediction? We evaluate label efficiency by training a linear probe on frozen MoRe representations to predict AMPS difficulty tiers (4 classes: arithmetic, algebra, calculus, advanced linear algebra), varying the number of labeled passages from 10 to 1,000. In the few-shot regime, all single-layer MoRe representations outperform PCA: MoRe_L2 achieves 80.0% at $n=10$ versus 77.0% for PCA (+3.9%), using only 64 dimensions from a single hierarchy layer compared to all 256 PCA components. MoRe_L2 at $n=50$ (84.5%, 64 dims) matches PCA at $n=100$ (84.8%, 256 dims), achieving equivalent performance with half the labeled data and one quarter the feature dimensions.

Summary of findings Across synthetic and real-world settings, MoRe consistently reuses previously learned structure, aligns shared components, and introduces new modules only when necessary. In controlled settings, this leads to accurate factor recovery and minimal forgetting, while in real-world data it produces interpretable hierarchical structure and improves label-efficient prediction.

6 Conclusion

We argued that the central challenge of continual learning is representational: incorporating new data with minimal interference requires a representation whose components reflect intrinsic structure in the data and can be selectively updated. We instantiated this view as MoRe, a framework that learns a hierarchical modular representation with identifiability guarantees from cross-layer time-delayed dependencies, paired with a two-phase adaptation procedure that interprets new data through existing modules and then selectively reuses, aligns, or expands them. Controlled synthetic experiments verify plasticity and stability across diverse transitions, and real-world LLM activations show that hierarchical structure emerges naturally and yields label-efficient representations.

Broader Impact. As foundational research, MoRe has no direct deployment path. Principled module reuse could lower the compute cost of adapting foundation models, broadening access; the interpretability of the learned hierarchy may also support auditing what a model has internalized. On the cautionary side, continually adapting systems can drift or entrench biases from skewed initial data—risks best mitigated by transparency and versioning of module libraries.

References

- [1] R. Aljundi, F. Babiloni, M. Elhoseiny, M. Rohrbach, and T. Tuytelaars. Memory aware synapses: Learning what (not) to forget. In *Proceedings of the European conference on computer vision (ECCV)*, pages 139–154, 2018.
- [2] R. Aljundi, P. Chakravarty, and T. Tuytelaars. Expert gate: Lifelong learning with a network of experts. In *Proceedings of the IEEE conference on computer vision and pattern recognition*, pages 3366–3375, 2017.
- [3] S. Biderman, H. Schoelkopf, Q. G. Anthony, H. Bradley, K. O’Brien, E. Hallahan, M. A. Khan, S. Purohit, U. S. Prashanth, E. Raff, et al. Pythia: A suite for analyzing large language models across training and scaling. In *International conference on machine learning*, pages 2397–2430. PMLR, 2023.
- [4] W. Chen, Y. Zhou, N. Du, Y. Huang, J. Laudon, Z. Chen, and C. Cui. Lifelong language pretraining with distribution-specialized experts. In *International Conference on Machine Learning*, pages 5383–5395. PMLR, 2023.
- [5] C. Fernando, D. Banarse, C. Blundell, Y. Zwols, D. Ha, A. A. Rusu, A. Pritzel, and D. Wierstra. Pathnet: Evolution channels gradient descent in super neural networks. *arXiv preprint arXiv:1701.08734*, 2017.
- [6] E. Fini, V. G. T. Da Costa, X. Alameda-Pineda, E. Ricci, K. Alahari, and J. Mairal. Self-supervised models are continual learners. In *Proceedings of the IEEE/CVF conference on computer vision and pattern recognition*, pages 9621–9630, 2022.
- [7] A. Gomez-Villa, B. Twardowski, L. Yu, A. D. Bagdanov, and J. Van de Weijer. Continually learning self-supervised representations with projected functional regularization. In *Proceedings of the IEEE/CVF conference on computer vision and pattern recognition*, pages 3867–3877, 2022.
- [8] N. Hounsby, A. Giurghi, S. Jastrzebski, B. Morrone, Q. De Laroussilhe, A. Gesmundo, M. Attariyan, and S. Gelly. Parameter-efficient transfer learning for nlp. In *International conference on machine learning*, pages 2790–2799. PMLR, 2019.
- [9] D. Hu, S. Yan, Q. Lu, L. Hong, H. Hu, Y. Zhang, Z. Li, X. Wang, and J. Feng. How well does self-supervised pre-training perform with streaming data? *arXiv preprint arXiv:2104.12081*, 2021.
- [10] E. J. Hu, Y. Shen, P. Wallis, Z. Allen-Zhu, Y. Li, S. Wang, L. Wang, W. Chen, et al. Lora: Low-rank adaptation of large language models. *Iclr*, 1(2):3, 2022.
- [11] J. Kirkpatrick, R. Pascanu, N. Rabinowitz, J. Veness, G. Desjardins, A. A. Rusu, K. Milan, J. Quan, T. Ramalho, A. Grabska-Barwinska, et al. Overcoming catastrophic forgetting in neural networks. *Proceedings of the national academy of sciences*, 114(13):3521–3526, 2017.
- [12] H. Li, S. Lin, L. Duan, Y. Liang, and N. B. Shroff. Theory on mixture-of-experts in continual learning. *arXiv preprint arXiv:2406.16437*, 2024.
- [13] Z. Li and D. Hoiem. Learning without forgetting. In B. Leibe, J. Matas, N. Sebe, and M. Welling, editors, *Computer Vision – ECCV 2016*, pages 614–629, Cham, 2016. Springer International Publishing.
- [14] Z. Li, Y. Shen, K. Zheng, R. Cai, X. Song, M. Gong, G. Chen, and K. Zhang. On the identification of temporal causal representation with instantaneous dependence. In *The Thirteenth International Conference on Learning Representations*, 2025.
- [15] Y.-S. Liang and W.-J. Li. Inflora: Interference-free low-rank adaptation for continual learning. In *Proceedings of the IEEE/CVF Conference on Computer Vision and Pattern Recognition*, pages 23638–23647, 2024.
- [16] W. Liu, F. Zhu, and C.-L. Liu. Branch-tuning: balancing stability and plasticity for continual self-supervised learning. *IEEE Transactions on Neural Networks and Learning Systems*, 2025.

- [17] C. Louizos, M. Welling, and D. P. Kingma. Learning sparse neural networks through l_0 regularization. *arXiv preprint arXiv:1712.01312*, 2017.
- [18] D. Madaan, J. Yoon, Y. Li, Y. Liu, and S. J. Hwang. Representational continuity for unsupervised continual learning. *arXiv preprint arXiv:2110.06976*, 2021.
- [19] A. Mallya and S. Lazebnik. Packnet: Adding multiple tasks to a single network by iterative pruning. In *Proceedings of the IEEE conference on Computer Vision and Pattern Recognition*, pages 7765–7773, 2018.
- [20] J. Pfeiffer, S. Ruder, I. Vulić, and E. M. Ponti. Modular deep learning. *arXiv preprint arXiv:2302.11529*, 2023.
- [21] E. M. Ponti, A. Sordani, Y. Bengio, and S. Reddy. Combining parameter-efficient modules for task-level generalisation. In *Proceedings of the 17th Conference of the European Chapter of the Association for Computational Linguistics*, pages 687–702, 2023.
- [22] D. Rao, F. Visin, A. Rusu, R. Pascanu, Y. W. Teh, and R. Hadsell. Continual unsupervised representation learning. *Advances in neural information processing systems*, 32, 2019.
- [23] S.-A. Rebuffi, A. Kolesnikov, G. Sperl, and C. H. Lampert. icarl: Incremental classifier and representation learning. In *Proceedings of the IEEE conference on Computer Vision and Pattern Recognition*, pages 2001–2010, 2017.
- [24] A. A. Rusu, N. C. Rabinowitz, G. Desjardins, H. Soyer, J. Kirkpatrick, K. Kavukcuoglu, R. Pascanu, and R. Hadsell. Progressive neural networks. *arXiv preprint arXiv:1606.04671*, 2016.
- [25] J. Serra, D. Suris, M. Miron, and A. Karatzoglou. Overcoming catastrophic forgetting with hard attention to the task. In *International conference on machine learning*, pages 4548–4557. PMLR, 2018.
- [26] N. Shazeer, A. Mirhoseini, K. Maziarz, A. Davis, Q. Le, G. Hinton, and J. Dean. Outrageously large neural networks: The sparsely-gated mixture-of-experts layer. *arXiv preprint arXiv:1701.06538*, 2017.
- [27] J. S. Smith, L. Karlinsky, V. Gutta, P. Cascante-Bonilla, D. Kim, A. Arbelle, R. Panda, R. Feris, and Z. Kira. Coda-prompt: Continual decomposed attention-based prompting for rehearsal-free continual learning. In *Proceedings of the IEEE/CVF conference on computer vision and pattern recognition*, pages 11909–11919, 2023.
- [28] X. Song, J. Sun, Z. Li, Y. Zheng, and K. Zhang. LLM interpretability with identifiable temporal-instantaneous representation. In *The Thirty-ninth Annual Conference on Neural Information Processing Systems*, 2025.
- [29] S. Tafazoli, F. M. Bouchacourt, A. Ardalan, N. T. Markov, M. Uchimura, M. G. Mattar, N. D. Daw, and T. J. Buschman. Building compositional tasks with shared neural subspaces. *Nature*, 650(8100):164–172, 2026.
- [30] C. I. Tang, L. Qendro, D. Spathis, F. Kawsar, C. Mascolo, and A. Mathur. Kaizen: Practical self-supervised continual learning with continual fine-tuning. In *Proceedings of the IEEE/CVF winter conference on applications of computer vision*, pages 2841–2850, 2024.
- [31] G. Team, T. Mesnard, C. Hardin, R. Dadashi, S. Bhupatiraju, S. Pathak, L. Sifre, M. Rivière, M. S. Kale, J. Love, et al. Gemma: Open models based on gemini research and technology. *arXiv preprint arXiv:2403.08295*, 2024.
- [32] K. Tian, Z. Zhao, Y. Chen, N. Ge, S. Cao, X. Han, J. Gu, and S. Yu. Domain-specific schema reuse supports flexible learning to learn in the primate brain. *Nature Communications*, 2026.
- [33] T. Veniat, L. Denoyer, and M. Ranzato. Efficient continual learning with modular networks and task-driven priors, 2021.

- [34] L. Wang, X. Zhang, H. Su, and J. Zhu. A comprehensive survey of continual learning: Theory, method and application. *IEEE transactions on pattern analysis and machine intelligence*, 46(8):5362–5383, 2024.
- [35] X. Wang, T. Chen, Q. Ge, H. Xia, R. Bao, R. Zheng, Q. Zhang, T. Gui, and X.-J. Huang. Orthogonal subspace learning for language model continual learning. In *Findings of the Association for Computational Linguistics: EMNLP 2023*, pages 10658–10671, 2023.
- [36] Z. Wang, Z. Zhang, S. Ebrahimi, R. Sun, H. Zhang, C.-Y. Lee, X. Ren, G. Su, V. Perot, J. Dy, et al. Dualprompt: Complementary prompting for rehearsal-free continual learning. In *European conference on computer vision*, pages 631–648. Springer, 2022.
- [37] Z. Wang, Z. Zhang, C.-Y. Lee, H. Zhang, R. Sun, X. Ren, G. Su, V. Perot, J. Dy, and T. Pfister. Learning to prompt for continual learning. In *Proceedings of the IEEE/CVF conference on computer vision and pattern recognition*, pages 139–149, 2022.
- [38] W. Yao, G. Chen, and K. Zhang. Temporally disentangled representation learning. *Advances in Neural Information Processing Systems*, 35:26492–26503, 2022.
- [39] J. Yu, Y. Zhuge, L. Zhang, P. Hu, D. Wang, H. Lu, and Y. He. Boosting continual learning of vision-language models via mixture-of-experts adapters. In *Proceedings of the IEEE/CVF Conference on Computer Vision and Pattern Recognition*, pages 23219–23230, 2024.
- [40] K. Zhang, S. Xie, I. Ng, and Y. Zheng. Causal representation learning from multiple distributions: A general setting. *arXiv preprint arXiv:2402.05052*, 2024.

Appendices for “MoRe: Modular Representations for Principled Continual Learning on LLMs”

Appendices Contents

A	Definitions and Proofs	13
A.1	Definitions	13
A.2	Proof for Theorem 1	14
A.3	Proof for Theorem 2	15
A.4	Proof for Corollary 1	16
A.5	Discussion of the Conditions	17
B	Implementation Details	17
B.1	Layer-wise Estimation	17
C	Adaptation Algorithm Details	19
C.1	Self-Consistency Score	19
C.2	Coordinate Expansion	19
C.3	Hard Concrete Gates	19
C.4	Loss Function	19
C.5	Algorithm	20
D	Limitations	20
E	Experimental Details	20
E.1	Synthetic Experiments	20
E.1.1	Layer-wise Estimation Results	20
E.2	Real-world Experiments on LLM Activations	22
E.2.1	Preprocessing of LLM Activations	22
E.2.2	S-RQ2&3 Settings	23
E.3	Transition scenarios	23
E.4	Hyperparameter selection	24
E.4.1	Extracted Low-to-High Layer Relations	24
F	Extended Related Work	24

A Definitions and Proofs

A.1 Definitions

Definition 1 ((Informal) Intimate Neighbor Set [14],[40]). *The intimate neighbor set of $V_i \in \mathbf{V}$ contains all such $V_j \in \mathbf{V}$ that are adjacent to V_i in the Markov network $\mathcal{M}_{\mathbf{V}}$ and also adjacent to all other neighbors of V_i .*

A.2 Proof for Theorem 1

Theorem 1 (Identifiability of Latent Variables). *Suppose the observed sequential data \mathbf{X}_t follows the data generating process with modular representations. Suppose the following two conditions C1 and C2 hold, then any mixture among \mathbf{Z} can only happen within the same layer. Furthermore, when C3 holds, \mathbf{Z} are component-wise identifiability.*

C1 (Smooth and Positive Density). *The conditional density $p(\mathbf{Z}_t | \mathbf{Z}_{t-1})$ is three times continuously differentiable and positive in \mathbf{R}^{md} .*

C2 (Sufficient Variability). *Let $\mathbf{W}_{t,i}^a \triangleq (\frac{\partial^2 \log p(\mathbf{Z}_t | \mathbf{Z}_{t-1})}{\partial Z_{t,i}^a \partial Z_{t-1,o}^{a'}})_{l' \in [d], o \in [m]}^\top$, for $i \in [m], a \in [d]$, $\mathbf{U}_{t,i}^a \triangleq (\frac{\partial^3 \log p(\mathbf{Z}_t | \mathbf{Z}_{t-1})}{\partial Z_{t,i}^a \partial Z_{t-1,o}^{a'} \partial Z_{t-1,o}^{a'}})_{l' \in [d], o \in [m]}^\top$ for $i \in [m], a \in [d]$, and $\mathbf{V}_{t,i,j}^a \triangleq (\frac{\partial^3 \log p(\mathbf{Z}_t | \mathbf{Z}_{t-1})}{\partial Z_{t,i}^a \partial Z_{t,j}^a \partial Z_{t-1,o}^{a'}})_{l' \in [d], o \in [m]}^\top$ for $i < j \in [m], a \in [d]$. For each value of \mathbf{Z}_t , all functions $\mathbf{W}_{t,1}^1, \mathbf{U}_{t,1}^1, \mathbf{V}_{t,1,2}^1, \dots, \mathbf{W}_{t,m}^d, \mathbf{U}_{t,m}^d, \mathbf{V}_{t,m-1,m}^d$ are linearly independent.*

C3 (Sparse Latent Process for Each Layer). *For any $Z_{t,i}^a$, either its intimate neighbor set is empty, or it has a child with empty intimate neighbor set.*

Proof. Assume the true model $(g, \{f_i\}_{i=1}^d, p(\epsilon_t))$ and the estimated model $(\hat{g}, \{\hat{f}_i\}_{i=1}^d, p(\hat{\epsilon}_t))$ induce the same distribution over the observations \mathbf{X}_t , and that both g and \hat{g} are invertible. Define the latent transformation

$$h \triangleq g^{-1} \circ \hat{g},$$

so that

$$\mathbf{Z}_t = h(\hat{\mathbf{Z}}_t).$$

Let

$$\mathbf{H}_t \triangleq \frac{\partial h(\hat{\mathbf{Z}}_t)}{\partial \hat{\mathbf{Z}}_t}$$

denote the Jacobian matrix of h evaluated at $\hat{\mathbf{Z}}_t$.

Step 1: Conditional density transformation. Consider the transformation $(\mathbf{X}_{t-1}, \hat{\mathbf{Z}}_t) \mapsto (\mathbf{X}_{t-1}, \mathbf{Z}_t)$. Its Jacobian is block triangular with determinant $|\det(\mathbf{H}_t)|$. Therefore,

$$p(\hat{\mathbf{Z}}_t, \mathbf{X}_{t-1}) = p(\mathbf{Z}_t, \mathbf{X}_{t-1}) |\det(\mathbf{H}_t)|.$$

Dividing both sides by $p(\mathbf{X}_{t-1})$ yields

$$p(\hat{\mathbf{Z}}_t | \mathbf{X}_{t-1}) = p(\mathbf{Z}_t | \mathbf{X}_{t-1}) |\det(\mathbf{H}_t)|.$$

Since $\mathbf{X}_{t-1} = g(\mathbf{Z}_{t-1}) = \hat{g}(\hat{\mathbf{Z}}_{t-1})$ and both mixing functions are invertible, we have

$$p(\mathbf{Z}_t | \mathbf{X}_{t-1}) = p(\mathbf{Z}_t | \mathbf{Z}_{t-1}), \quad p(\hat{\mathbf{Z}}_t | \mathbf{X}_{t-1}) = p(\hat{\mathbf{Z}}_t | \hat{\mathbf{Z}}_{t-1}).$$

Thus,

$$\log p(\hat{\mathbf{Z}}_t | \hat{\mathbf{Z}}_{t-1}) = \log p(\mathbf{Z}_t | \mathbf{Z}_{t-1}) + \log |\det(\mathbf{H}_t)|. \quad (6)$$

Step 2: Cross-layer conditional independence. By the modular representation assumption, there are no instantaneous dependencies across different layers. Hence for any $b \neq b'$ and any k, l ,

$$\frac{\partial^2}{\partial \hat{Z}_{t,k}^b \partial \hat{Z}_{t,l}^{b'}} \log p(\hat{\mathbf{Z}}_t | \hat{\mathbf{Z}}_{t-1}) = 0.$$

Applying this to Eq. (6), we obtain

$$\frac{\partial^2 \log p(\mathbf{Z}_t | \mathbf{Z}_{t-1})}{\partial \hat{Z}_{t,k}^b \partial \hat{Z}_{t,l}^{b'}} + \frac{\partial^2 \log |\det(\mathbf{H}_t)|}{\partial \hat{Z}_{t,k}^b \partial \hat{Z}_{t,l}^{b'}} = 0. \quad (7)$$

Step 3: Chain rule expansion. Using the chain rule,

$$\frac{\partial^2 \log p(\mathbf{Z}_t | \mathbf{Z}_{t-1})}{\partial \hat{Z}_{t,k}^b \partial \hat{Z}_{t,l}^{b'}} = \sum_{i,a} \frac{\partial \log p(\mathbf{Z}_t | \mathbf{Z}_{t-1})}{\partial Z_{t,i}^a} \frac{\partial^2 Z_{t,i}^a}{\partial \hat{Z}_{t,k}^b \partial \hat{Z}_{t,l}^{b'}} \quad (8)$$

$$+ \sum_{i,a} \sum_{j,a'} \frac{\partial^2 \log p(\mathbf{Z}_t | \mathbf{Z}_{t-1})}{\partial Z_{t,i}^a \partial Z_{t,j}^{a'}} \frac{\partial Z_{t,i}^a}{\partial \hat{Z}_{t,k}^b} \frac{\partial Z_{t,j}^{a'}}{\partial \hat{Z}_{t,l}^{b'}}. \quad (9)$$

By modularity, cross-layer second derivatives vanish for $a \neq a'$, hence only terms with $a = a'$ remain. Rewriting the second sum symmetrically over $i < j$, we obtain

$$\sum_{i,a} \frac{\partial \log p(\mathbf{Z}_t | \mathbf{Z}_{t-1})}{\partial Z_{t,i}^a} \frac{\partial^2 Z_{t,i}^a}{\partial \hat{Z}_{t,k}^b \partial \hat{Z}_{t,l}^{b'}} \quad (10)$$

$$+ \sum_{i,a} \frac{\partial^2 \log p(\mathbf{Z}_t | \mathbf{Z}_{t-1})}{\partial (Z_{t,i}^a)^2} \frac{\partial Z_{t,i}^a}{\partial \hat{Z}_{t,k}^b} \frac{\partial Z_{t,i}^a}{\partial \hat{Z}_{t,l}^{b'}} \quad (11)$$

$$+ \sum_{i < j, a} \frac{\partial^2 \log p(\mathbf{Z}_t | \mathbf{Z}_{t-1})}{\partial Z_{t,i}^a \partial Z_{t,j}^a} \left(\frac{\partial Z_{t,i}^a}{\partial \hat{Z}_{t,k}^b} \frac{\partial Z_{t,j}^a}{\partial \hat{Z}_{t,l}^{b'}} + \frac{\partial Z_{t,j}^a}{\partial \hat{Z}_{t,k}^b} \frac{\partial Z_{t,i}^a}{\partial \hat{Z}_{t,l}^{b'}} \right). \quad (12)$$

Step 4: Differentiation w.r.t. lagged variables. Since \mathbf{H}_t depends only on $\hat{\mathbf{Z}}_t$, we have

$$\frac{\partial}{\partial Z_{t-1,o}'} \log |\det(\mathbf{H}_t)| = 0.$$

Differentiating Eq. (7) with respect to $Z_{t-1,o}'$ eliminates the Jacobian term, yielding

$$(\text{linear combination of } \mathbf{W}_{t,i}^a, \mathbf{U}_{t,i}^a, \mathbf{V}_{t,i,j}^a) \equiv 0. \quad (13)$$

Step 5: Apply sufficient variability (C2). By Condition C2, the collection of vectors

$$\{\mathbf{W}_{t,i}^a, \mathbf{U}_{t,i}^a, \mathbf{V}_{t,i,j}^a\}$$

is linearly independent. Therefore, all coefficients in Eq. (13) must vanish. This implies:

$$\begin{aligned} \frac{\partial^2 Z_{t,i}^a}{\partial \hat{Z}_{t,k}^b \partial \hat{Z}_{t,l}^{b'}} &= 0, \\ \frac{\partial Z_{t,i}^a}{\partial \hat{Z}_{t,k}^b} \frac{\partial Z_{t,i}^a}{\partial \hat{Z}_{t,l}^{b'}} &= 0, \\ \frac{\partial Z_{t,i}^a}{\partial \hat{Z}_{t,k}^b} \frac{\partial Z_{t,j}^a}{\partial \hat{Z}_{t,l}^{b'}} + \frac{\partial Z_{t,j}^a}{\partial \hat{Z}_{t,k}^b} \frac{\partial Z_{t,i}^a}{\partial \hat{Z}_{t,l}^{b'}} &= 0, \end{aligned}$$

for all (i, j) with $i < j$.

Step 6: Conclusion. These constraints imply that each ground-truth latent variable depends only on estimated latent variables from a single layer, and no mixing across layers is possible.

The remaining ambiguity within each layer is resolved by existing results (e.g., Theorem 1 and Theorem 3 in [14]), which show that under C3, the latent variables are component-wise identifiable. In the absence of instantaneous dependencies, the result reduces to the setting of [38]. \square

A.3 Proof for Theorem 2

Theorem 2 (Identifiability of Hierarchical Order). *Suppose the observed sequential data \mathbf{X}_t follows the data-generating process with modular representations. Suppose the assumptions of Theorem 1 hold. Suppose further that:*

C4 (Hierarchical Mask Constraint). The estimated transition model is constrained by a layer-wise hierarchical mask: under an estimated order $\hat{\pi}$, time-delayed effects from layer a to layer b are allowed only if $\hat{\pi}^{-1}(a) < \hat{\pi}^{-1}(b)$.

C5 (Unique Compatible Order). The true layer-level time-delayed graph admits a unique compatible order.

Then any estimated hierarchical order that induces the same observational distribution as the true model must be compatible with the true layer-level time-delayed graph. In particular, the hierarchy is identifiable up to compatible order. Moreover, under C5, the hierarchical order is uniquely identifiable.

Proof. By Theorem 1, any admissible transformation between the true latent variables and the estimated latent variables is block-wise with respect to layers. Therefore, estimated latent variables from one layer can correspond only to true latent variables from one layer, up to a permutation of layers and possible within-layer transformations.

It remains to determine which permutations of the layers are admissible. Let $\hat{\pi}$ be an estimated hierarchical order that induces the same observational distribution as the true data-generating process. Suppose, for contradiction, that $\hat{\pi}$ is not compatible with the true layer-level time-delayed graph \mathcal{G}_{lag} . Then there exists an edge

$$(a, b) \in \mathcal{E}_{\text{lag}}$$

such that

$$\hat{\pi}^{-1}(a) > \hat{\pi}^{-1}(b).$$

In the true process, the edge (a, b) means that the past layer \mathbf{Z}_{t-1}^a has a nonzero time-delayed effect on the current layer \mathbf{Z}_t^b .

However, under the estimated order $\hat{\pi}$, layer a is placed after layer b . By the hierarchical mask constraint C4, the estimated model forbids any time-delayed effect from layer a to layer b . Therefore, the estimated model cannot represent the true time-delayed dependence from \mathbf{Z}_{t-1}^a to \mathbf{Z}_t^b .

This contradicts the assumption that the estimated model induces the same observational distribution as the true model. Hence no such violating edge can exist, and every admissible estimated order $\hat{\pi}$ must satisfy

$$(a, b) \in \mathcal{E}_{\text{lag}} \implies \hat{\pi}^{-1}(a) < \hat{\pi}^{-1}(b).$$

Thus, $\hat{\pi}$ is a compatible order of \mathcal{G}_{lag} .

Therefore, the hierarchy is identifiable up to the set of compatible orders

$$\text{Top}(\mathcal{G}_{\text{lag}}).$$

If C5 holds, then \mathcal{G}_{lag} has a unique compatible order. Hence the estimated order must equal this unique order, and the hierarchical order is identifiable. \square

A.4 Proof for Corollary 1

Corollary 1 (Identifiability of the Latent Process). *Suppose the observed sequential data \mathbf{X}_t follows the data-generating process with modular representations. Suppose the assumptions of Theorem 1 and Theorem 2 hold. Suppose further that the latent variables are within-layer component-wise identifiable, for example by [14]. Then the full latent process is identifiable up to compatible hierarchical order. If C5 holds, then the full latent process is identifiable up to the remaining component-wise indeterminacies.*

Proof. By Theorem 1, no admissible transformation can mix latent variables across different layers. Hence the layer partition is identifiable up to a permutation of layers.

By the assumed within-layer component-wise identifiability, the remaining ambiguity inside each layer is removed up to the standard component-wise indeterminacies. Therefore, the latent variables are identifiable layer by layer.

By Theorem 2, the layer ordering is identifiable up to compatible order. Hence the latent process, including the layer partition, the component-wise latent variables within each layer, and the layer-level time-delayed structure, is identifiable up to compatible hierarchical order.

If C5 holds, the compatible hierarchical order is unique. Therefore, the entire modular latent process is identifiable up to the remaining component-wise indeterminacies inherited from the within-layer identifiability result. \square

A.5 Discussion of the Conditions

B Implementation Details

B.1 Layer-wise Estimation

We give the implementation details for the progressive estimator used when the joint objective in Eq. (3) is too expensive to optimize. Throughout this subsection, let $x_t := X_t^{\text{proj}}$ denote the projected observation used by the encoder. We index layers in the order in which they are estimated: layer 1 is the first, most fundamental module, and layer i is estimated after layers $1, \dots, i-1$ have been recovered. This notation matches the estimation order; if the generative-model section uses the reverse topological convention, the indices here should be interpreted after topological sorting of the layer-level time-delayed graph.

Principle. The layer-wise estimator follows directly from the hierarchical restriction in Eq. (2). Once $\hat{Z}_t^{<i} := (\hat{Z}_t^1, \dots, \hat{Z}_t^{i-1})$ has been learned, these earlier modules are treated as anchors. The next encoder f_i is trained so that $\hat{Z}_t^i = f_i(x_t)$ is (i) informative about the part of x_t not yet explained by previous modules, (ii) predictive from the allowed delayed parents $(\hat{Z}_{t-1}^i, \hat{Z}_{t-1}^{<i})$, and (iii) conditionally independent of the raw past observation once these allowed parents are known. The last condition prevents the new layer from hiding information that should have been captured by the already learned layers.

First-layer objective. For the first layer, define $\hat{Z}_t^1 = f_1(x_t)$. We use two conditional density models with matched architecture and noise prior,

$$q_1^0(\hat{z}_t^1 | \hat{z}_{t-1}^1), \quad q_1^1(\hat{z}_t^1 | \hat{z}_{t-1}^1, x_{t-1}), \quad (14)$$

where q_1^0 is the admissible first-layer temporal model and q_1^1 is an augmented model that also sees the raw past. The conditional-independence requirement

$$\hat{Z}_t^1 \perp\!\!\!\perp X_{t-1} | \hat{Z}_{t-1}^1 \quad (15)$$

is enforced by the density-ratio estimate

$$\mathcal{L}_{\text{cmi}}^1 = \mathbb{E}_t \left[\log q_1^1(\hat{Z}_t^1 | \hat{Z}_{t-1}^1, x_{t-1}) - \log q_1^0(\hat{Z}_t^1 | \hat{Z}_{t-1}^1) \right]. \quad (16)$$

Minimizing Eq. (16) discourages any additional predictive information in x_{t-1} beyond \hat{Z}_{t-1}^1 . To avoid collapse, we combine this term with an informativeness loss and a temporal prediction loss. In our implementation, the informativeness term is a reconstruction loss

$$\mathcal{L}_{\text{rec}}^1 = \mathbb{E}_t \left[\|x_t - \tilde{g}_1(\hat{Z}_t^1)\|_2^2 \right], \quad (17)$$

and the prediction term is a JEPA-style loss with an exponential-moving-average target encoder \bar{f}_1 ,

$$\mathcal{L}_{\text{pred}}^1 = \mathbb{E}_t \left[\|r_1(\hat{Z}_{t-1}^1) - \text{sg}(\bar{f}_1(x_t))\|_2^2 \right], \quad (18)$$

where r_1 is a latent predictor and $\text{sg}(\cdot)$ denotes stop-gradient. A variance floor

$$\mathcal{L}_{\text{var}}^1 = \sum_k \max\{0, \rho - \text{Std}(\hat{Z}_{t,k}^1)\} \quad (19)$$

is optionally used to rule out degenerate constant representations.

Conditional-density instantiation. The density models q_i^0 and q_i^1 can be implemented either as conditional normalizing flows or as Gaussian conditional density heads. For a flow implementation, with context c_t^0 , we write

$$e_t = T_\phi(\hat{z}_t^i; c_t^0), \quad \log q_\phi(\hat{z}_t^i | c_t^0) = \log p_E(e_t) + \log \left| \det \frac{\partial T_\phi(\hat{z}_t^i; c_t^0)}{\partial \hat{z}_t^i} \right|. \quad (20)$$

For the Gaussian-head implementation, $q_\phi(\hat{z} | c) = \mathcal{N}(\mu_\phi(c), \text{diag } \sigma_\phi^2(c))$. In both cases, q_i^0 and q_i^1 must share the same density family and noise prior; otherwise, the difference $\log q_i^1 - \log q_i^0$ could reflect extra flexibility rather than additional information in the raw past.

Recursive estimation of later layers. After estimating layers $< i$, we freeze f_1, \dots, f_{i-1} and learn only f_i , its decoder head, its predictor, and its density models. Define the admissible context

$$c_{i,t}^0 := (\hat{Z}_{t-1}^i, \hat{Z}_{t-1}^{<i}), \quad (21)$$

which contains the previous value of the new layer and the delayed values of all already recovered modules. The augmented context is

$$c_{i,t}^1 := (\hat{Z}_{t-1}^i, \hat{Z}_{t-1}^{<i}, x_{t-1}). \quad (22)$$

The layer- i CMI penalty is then

$$\mathcal{L}_{\text{cmi}}^i = \mathbb{E}_t \left[\log q_t^1(\hat{Z}_t^i | c_{i,t}^1) - \log q_t^0(\hat{Z}_t^i | c_{i,t}^0) \right], \quad (23)$$

which estimates $I(\hat{Z}_t^i; X_{t-1} | \hat{Z}_{t-1}^i, \hat{Z}_{t-1}^{<i})$. The reconstruction term is applied to the full representation recovered so far,

$$\mathcal{L}_{\text{rec}}^i = \mathbb{E}_t \left[\|x_t - \tilde{g}_i(\hat{Z}_t^{<i})\|_2^2 \right], \quad \hat{Z}_t^{<i} = (\hat{Z}_t^{<i}, \hat{Z}_t^i), \quad (24)$$

with previous encoders frozen. This allows the decoder to change while preventing later layers from overwriting earlier modules. When desired, one can further residualize the input by replacing x_t with $x_t - \tilde{g}_{i-1}(\hat{Z}_t^{<i})$, but our experiments use the full-observation decoder for stability.

The complete layer- i encoder objective is

$$\mathcal{L}_i = \lambda_{\text{rec}} \mathcal{L}_{\text{rec}}^i + \lambda_{\text{pred}} \mathcal{L}_{\text{pred}}^i + \lambda_{\text{cmi}} \mathcal{L}_{\text{cmi}}^i + \lambda_0 \mathcal{L}_0^i + \lambda_1 \mathcal{L}_1^i + \lambda_{\text{var}} \mathcal{L}_{\text{var}}^i + \lambda_{\text{orth}} \mathcal{L}_{\text{orth}}^i, \quad (25)$$

where

$$\mathcal{L}_0^i = -\mathbb{E}_t \log q_t^0(\hat{Z}_t^i | c_{i,t}^0), \quad \mathcal{L}_1^i = -\mathbb{E}_t \log q_t^1(\hat{Z}_t^i | c_{i,t}^1). \quad (26)$$

The optional decorrelation term

$$\mathcal{L}_{\text{orth}}^i = \sum_{j < i} \left\| \text{Cov}(\hat{Z}_t^i, \hat{Z}_t^j) \right\|_F^2 \quad (27)$$

helps avoid relearning an already recovered module, but it is not required by the theory because the main hierarchy constraint is imposed through the delayed contexts in Eq. (23).

Optimization schedule. For each layer, we alternate two updates. First, with encoder outputs detached, we fit the density estimators by minimizing $\mathcal{L}_0^i + \mathcal{L}_1^i$. Second, with the density estimators fixed, we update f_i using Eq. (25). In practice, we warm up the encoder with $\mathcal{L}_{\text{pred}} + \mathcal{L}_{\text{rec}}$ before enabling the CMI penalty. This warm-up prevents early density-estimation noise from collapsing the representation. After warm-up, the prediction loss can be hinge-thresholded at the warm-up value so that the CMI term shapes the representation without sacrificing temporal predictability.

Layer-wise estimator. Algorithm 1 summarizes the recursive procedure.

Algorithm 1 Layer-wise estimation on the initial dataset

Require: Initial dataset $D_0 = \{x_t\}_{t=1}^T$, number of layers d , layer dimensions m_i , lag L , loss weights λ .

- 1: Fit the projection basis (V_0, μ_0) and set $x_t = (X_t - \mu_0)V_0$
 - 2: Initialize the learned module list $\mathcal{M} \leftarrow \emptyset$
 - 3: **for** $i = 1, \dots, d$ **do**
 - 4: Freeze all encoders in \mathcal{M} ; compute $\hat{Z}_t^{<i}$ for all t
 - 5: Initialize f_i , decoder \tilde{g}_i , predictor r_i , target encoder \bar{f}_i , and density models (q_i^0, q_i^1)
 - 6: **for** training epochs **do**
 - 7: Form $\hat{Z}_t^i = f_i(x_t)$, admissible context $c_{i,t}^0$, and augmented context $c_{i,t}^1$
 - 8: Update (q_i^0, q_i^1) with \hat{Z}_t^i detached by minimizing $\mathcal{L}_0^i + \mathcal{L}_1^i$
 - 9: Update f_i, \tilde{g}_i, r_i by minimizing Eq. (25)
 - 10: Update the target encoder $\bar{f}_i \leftarrow \tau f_i + (1 - \tau) \bar{f}_i$
 - 11: **end for**
 - 12: Add f_i to \mathcal{M} and estimate the new transition block from $(\hat{Z}_{t-1}^{<i}, \hat{Z}_t^{<i})$
 - 13: **end for**
 - 14: **return** Encoder $f = (f_1, \dots, f_d)$, decoder \tilde{g}_d , transition estimate J_B , and projection basis (V_0, μ_0)
-

C Adaptation Algorithm Details

We provide the implementation details of the adaptation procedure introduced in Section 4.2. Our experiments use a linear instantiation: f_{k-1} is parameterized by $\mathbf{F}_{k-1} \in \mathbb{R}^{d_{k-1} \times m_{k-1}}$ and the alignment T by $\mathbf{T} \in \mathbb{R}^{m_{k-1} \times m_{k-1}}$.

C.1 Self-Consistency Score

Given the inference-only forward pass $\mathbf{Z}_{t-1} = \mathbf{X}_{t-1}^{\text{proj}} \mathbf{F}_{k-1}$, $\mathbf{Z}_t = \mathbf{X}_t^{\text{proj}} \mathbf{F}_{k-1}$, and residuals $\mathbf{E}_t = \mathbf{Z}_t - \mathbf{Z}_{t-1} \mathbf{J}_B^{(k-1)\top}$, define the correlation matrices

$$\mathbf{H}_1[i, j] = \text{corr}(E_{i,t}, Z_{j,t-1}), \quad \mathbf{H}_3[i, j] = \text{corr}(Z_{i,t-1}, Z_{j,t}). \quad (28)$$

The self-consistency score is

$$a_j = |\mathbf{H}_3[j, j]| \cdot \left(1 - \frac{1}{m-1} \sum_{i \neq j} |\mathbf{H}_1[i, j]|\right), \quad a_j \in [0, 1]. \quad (29)$$

Candidate new modules are assigned $a_j = 0$.

C.2 Coordinate Expansion

The residual $\mathbf{R} = \mathbf{X}_k - (\mathbf{X}^{\text{proj}} \mathbf{V}_{k-1}^\top + \boldsymbol{\mu}_{k-1})$ is centered, and its top k_{extra} right singular vectors are orthogonalized against \mathbf{V}_{k-1} (Gram-Schmidt), then orthonormalized via thin QR, yielding $\mathbf{V}^{\text{new}} \in \mathbb{R}^{n \times k_{\text{extra}}}$ with $\mathbf{V}^{\text{new}\top} \mathbf{V}_{k-1} = \mathbf{0}$. The transition is extended as

$$\mathbf{J}_B^{\text{ext}} = \begin{bmatrix} \mathbf{J}_B^{(k-1)} & \mathbf{0} \\ \mathbf{J}_B^{\text{old} \rightarrow \text{new}} & \mathbf{J}_B^{\text{new} \rightarrow \text{new}} \end{bmatrix}, \quad (30)$$

with the zero block enforcing the layer-wise hierarchy mask of Theorem 2.

C.3 Hard Concrete Gates

Each gate $g_j \in [0, 1]$ has logit ℓ_j and is sampled during training as

$$g_j = \text{clip}_{[0,1]}(\bar{s}), \quad \bar{s} = s(\zeta - \gamma) + \gamma, \quad s = \sigma\left(\frac{\log u - \log(1-u) + \ell_j}{\tau}\right), \quad u \sim \text{Uniform}(0, 1), \quad (31)$$

with $\zeta = 1.1$, $\gamma = -0.1$, and τ annealed from τ_{start} to τ_{end} . At evaluation, $g_j = \mathbb{1}[\sigma(\ell_j) > 0.5]$. The expected L_0 regularizer is

$$\mathcal{L}_0(\mathbf{g}) = \sum_j \sigma(\ell_j - \tau \log(-\gamma/\zeta)). \quad (32)$$

Logits for existing modules are initialized from \mathbf{a} as

$$\ell_j = C \cdot (2 \text{softmax}_T(\mathbf{a})_j - 1) \cdot \text{clip}(\bar{a}/\eta, 0, 1), \quad \bar{a} = \frac{1}{m_{k-1}} \sum_j a_j, \quad (33)$$

with hyperparameters C, T, η . Logits for candidate new modules are initialized at 0.

C.4 Loss Function

In the linear instantiation, the data loss is

$$\mathcal{L}_{\text{data}} = \|\mathbf{E}_t\|_1 - \frac{1}{2} \log \det(\mathbf{F}^{\text{active}, \top} \mathbf{F}^{\text{active}} + \varepsilon \mathbf{I}), \quad (34)$$

where $\mathbf{F}^{\text{active}} = [\mathbf{F}_{k-1} \mathbf{T} \cdot \text{diag}(\mathbf{g}^{\text{old}}), \mathbf{F}^{\text{new}}]$. The alignment regularizer is $\mathcal{R}(\mathbf{T}) = \|\mathbf{T} - \mathbf{I}\|_F^2$. The full objective is

$$\mathcal{L}_{\text{adapt}} = \mathcal{L}_{\text{data}} + \lambda_{\text{align}} \mathcal{R}(\mathbf{T}) + \lambda_{\text{sp}}^{\text{old}} \mathcal{L}_0(\mathbf{g}^{\text{old}}) + \lambda_{\text{sp}}^{\text{new}} \mathcal{L}_0(\mathbf{g}^{\text{new}}) + \lambda_J (\|\mathbf{J}_B^{\text{old} \rightarrow \text{new}}\|_1 + \|\mathbf{J}_B^{\text{new} \rightarrow \text{new}}\|_1). \quad (35)$$

C.5 Algorithm

Algorithm 2 MoRe Continual Adaptation at Stage k

Require: \mathcal{D}_k ; previous $\mathbf{F}_{k-1}, \mathbf{V}_{k-1}, \boldsymbol{\mu}_{k-1}, \mathbf{J}_B^{(k-1)}$
Require: Hyperparameters $\{\lambda, C, T, \eta\}$, warmup fraction r , epochs N , expansion budget k_{extra}

// Phase 1: Fitting and Assessment

- 1: $\mathbf{X}^{\text{proj}} \leftarrow (\mathbf{X}_k - \boldsymbol{\mu}_{k-1})\mathbf{V}_{k-1}$
- 2: Compute $\mathbf{Z}_{t-1}, \mathbf{Z}_t, \mathbf{E}_t, \mathbf{H}_1, \mathbf{H}_3$ ▷ inference only
- 3: $a_j \leftarrow |\mathbf{H}_3[j, j]| \cdot \left(1 - \frac{1}{m-1} \sum_{i \neq j} |\mathbf{H}_1[i, j]|\right)$
- 4: $\mathbf{V}^{\text{new}} \leftarrow$ orthogonalized top- k_{extra} singular vectors of residual \mathbf{R}
- 5: Allocate $\mathbf{F}^{\text{new}}, \mathbf{J}_B^{\text{old} \rightarrow \text{new}}, \mathbf{J}_B^{\text{new} \rightarrow \text{new}}, \mathbf{T} \leftarrow \mathbf{I}$
- 6: Initialize ℓ^{old} from \mathbf{a} ; $\ell^{\text{new}} \leftarrow \mathbf{0}$

// Phase 2: Selective Updating

- 7: **for** epoch = 1 **to** N **do**
- 8: Anneal τ ; sample $\mathbf{g}^{\text{old}}, \mathbf{g}^{\text{new}}$ via Hard Concrete
- 9: Compute $\mathcal{L}_{\text{adapt}}$; update $\mathbf{T}, \mathbf{F}^{\text{new}}, \mathbf{J}_B^{\text{old} \rightarrow \text{new}}, \mathbf{J}_B^{\text{new} \rightarrow \text{new}}$
- 10: **if** epoch > $r \cdot N$ **then**
- 11: Update gate logits $\ell^{\text{old}}, \ell^{\text{new}}$
- 12: **end if**
- 13: **end for**

// Commit

- 14: Binarize: $g_j \leftarrow \mathbb{1}[\sigma(\ell_j) > 0.5]$
- 15: $\mathbf{V}_k \leftarrow [\mathbf{V}_{k-1}, \mathbf{V}^{\text{new}}[:, \mathbf{g}^{\text{new}} = 1]]$
- 16: $\mathbf{F}_k \leftarrow [\mathbf{F}_{k-1}\mathbf{T}, \mathbf{F}^{\text{new}}[:, \mathbf{g}^{\text{new}} = 1]]$
- 17: Assemble $\mathbf{J}_B^{(k)}$ from $\mathbf{J}_B^{(k-1)}$ and selected new blocks
- 18: Store $\mathbf{g}^{(k)}$

Ensure: $(\mathbf{V}_k, \boldsymbol{\mu}_{k-1}, \mathbf{F}_k, \mathbf{J}_B^{(k)}, \mathbf{g}^{(k)})$

D Limitations

Our experiments are designed primarily as concept verification rather than benchmark competition. The synthetic settings, while controlled and informative for isolating mechanism, cover a limited range of transitions, dimensionalities, and noise structures; the real-world LLM activation experiments are similarly scoped to demonstrate the emergence of hierarchical structure rather than to claim downstream gains across diverse tasks. The implementation evaluated here uses a linear instantiation of the framework, which is principled but restrictive: scaling to nonlinear encoders, longer adaptation chains, and richer real-world distribution shifts is left to future work. Several theoretical assumptions—unidirectional cross-layer time-delayed structure, sufficient variability, and within-layer sparsity—may be only approximately satisfied in practice, and a systematic study of robustness to such violations remains open. Finally, our method addresses one adaptation step at a time; long-horizon stability across many sequential stages, and the design of memory mechanisms for reactivating long-dormant modules, are natural next steps toward a complete continual learning system.

E Experimental Details

E.1 Synthetic Experiments

E.1.1 Layer-wise Estimation Results

We focus especially on first-layer estimation because, in the layer-wise estimator, accurate recovery of the initial layer provides the anchor for estimating subsequent layers. Once an earlier layer has been recovered, the same estimation principle can be applied recursively to later layers by conditioning on the already learned lower-level structure. The experiments below therefore test whether the learned scalar representation preferentially aligns with ground-truth first-layer coordinates, and whether this

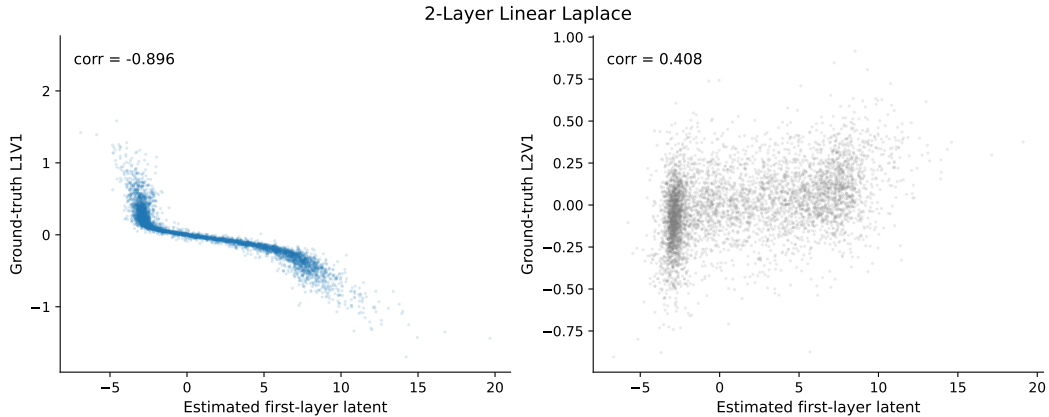


Figure 5: Two-layer linear non-Gaussian synthetic experiment. Each panel plots the learned scalar first-layer representation against one ground-truth latent coordinate. The left panel shows strong alignment with the first-layer latent, while the right panel shows a noticeably weaker relationship with the second-layer latent.

behavior persists when the generator becomes nonlinear and when the hierarchy is extended to three layers.

We next visualize first-layer estimation on synthetic temporal data. In all panels, the horizontal axis is the learned scalar first-layer representation, while the vertical axis is a ground-truth latent coordinate from the synthetic generator. Because recovered latent coordinates are identifiable only up to the usual component-wise indeterminacies, and up to sign and scaling in the scalar linear diagnostics considered here, we report absolute correlations; a strong negative correlation is therefore as meaningful as a strong positive one. The main diagnostic question is whether the learned representation aligns more strongly with first-layer latents than with deeper-layer latents.

Figure 5 shows the two-layer linear non-Gaussian case. The learned representation exhibits a strong monotone relationship with the true first-layer latent and a substantially weaker relationship with the second-layer latent. Quantitatively, the final absolute correlation with the first-layer latent is about 0.90, versus about 0.41 for the second-layer latent. This is the expected qualitative pattern for successful first-layer recovery: the representation tracks the first layer closely while remaining relatively insensitive to the other latent coordinate.

Figure 6 reports the corresponding two-layer nonlinear setting. The same qualitative pattern persists, but the first-layer alignment becomes even stronger: the final absolute correlation with the first-layer latent is about 0.97, while the second-layer correlation remains around 0.42. This indicates that the method is not restricted to the linear case and can still isolate the first layer when the latent dynamics and/or observation mapping become nonlinear.

For the more challenging three-layer setting with two latent variables per layer, Figures 7 and 8 provide two complementary views. Figure 7 concentrates on the two first-layer coordinates. One coordinate is recovered very strongly ($|corr| \approx 0.94$), while the other is recovered more moderately ($|corr| \approx 0.49$). This is consistent with the current estimator being one-dimensional: it captures one dominant direction in the first-layer subspace, but it does not reconstruct the full two-dimensional first-layer subspace.

Figure 8 expands the same comparison to all six latent coordinates. The dominant first-layer coordinate still yields the largest absolute correlation, which is the key sign of first-layer recovery. At the same time, some non-first-layer coordinates remain substantially correlated, especially one coordinate in the third layer. We therefore interpret the three-layer result as a partial but meaningful success: the estimator continues to prioritize the first layer, but the separation from the remaining latent coordinates is no longer as clean as in the simpler two-layer case.

Overall, these four figures support a cautious version of the intended conclusion. In the two-layer settings, the learned scalar representation aligns much more strongly with the first-layer latent than with the second-layer latent, under both linear Laplace and nonlinear Laplace data generation. In the

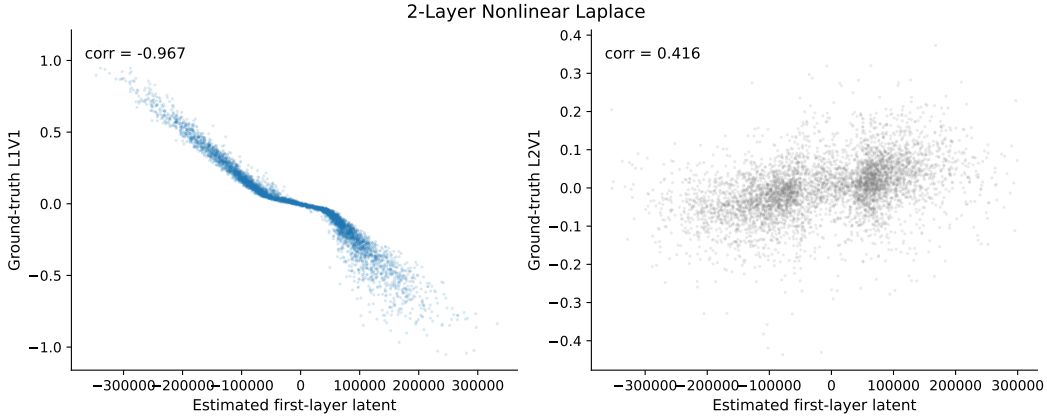


Figure 6: Two-layer nonlinear synthetic experiment. The learned representation remains strongly aligned with the first-layer latent and only weakly aligned with the second-layer latent, showing that the first-layer recovery pattern persists beyond the linear setting.

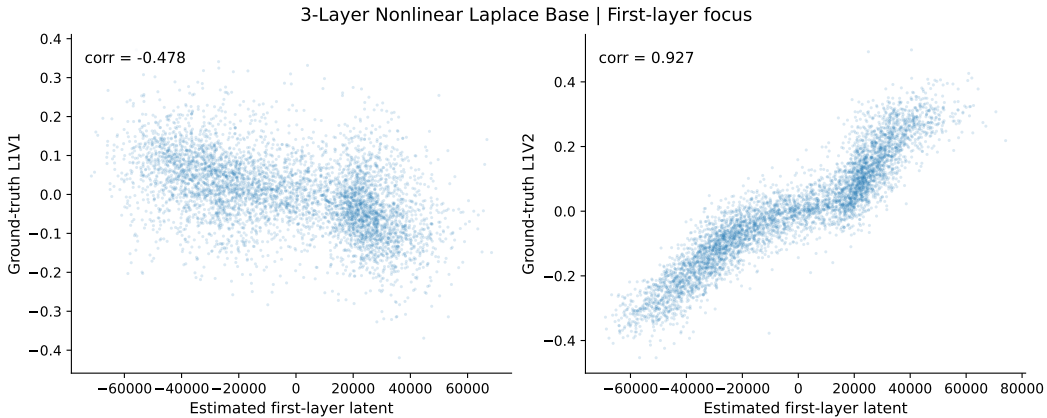


Figure 7: Three-layer synthetic experiment, first-layer focus. The learned scalar representation is plotted against the two first-layer ground-truth coordinates. The estimator strongly captures one dominant first-layer direction, while the second first-layer coordinate is represented more weakly.

harder three-layer setting, the largest absolute correlation is still attained by a first-layer coordinate, but one third-layer coordinate and one second-layer coordinate remain substantially correlated. Thus, the three-layer experiment provides evidence of preferential first-layer estimation in a deeper hierarchy, rather than full separation of all layers or full recovery of the two-dimensional first-layer subspace.

E.2 Real-world Experiments on LLM Activations

E.2.1 Preprocessing of LLM Activations

LLM Activations We extract hidden-state activations from two pretrained language models, namely, Pythia-1.4B and Gemma-2-9B, by registering forward hooks at a single intermediate layer (layer 16 and layer 25 respectively), chosen to capture rich semantic representations at approximately 60% of network depth. For each dataset, we stream up to 50,000 passages (arXiv title+abstract concatenations, AMPS problem+solution pairs, Wikipedia articles), tokenize and truncate to 512 tokens, and run the frozen LLM to extract per-token hidden states, i.e., activations. The resulting token-level activation hidden dimension of Pythia-1.4B and Gemma-2-9B are 2048 and 3584 respectively. They are compressed to 256 dimensions via Incremental PCA separately. Consecutive token windows of length $p + 1$ are constructed within passage boundaries to form training samples for MoRe, preserving local sequential structure without crossing document boundaries. We set the number of hierarchy

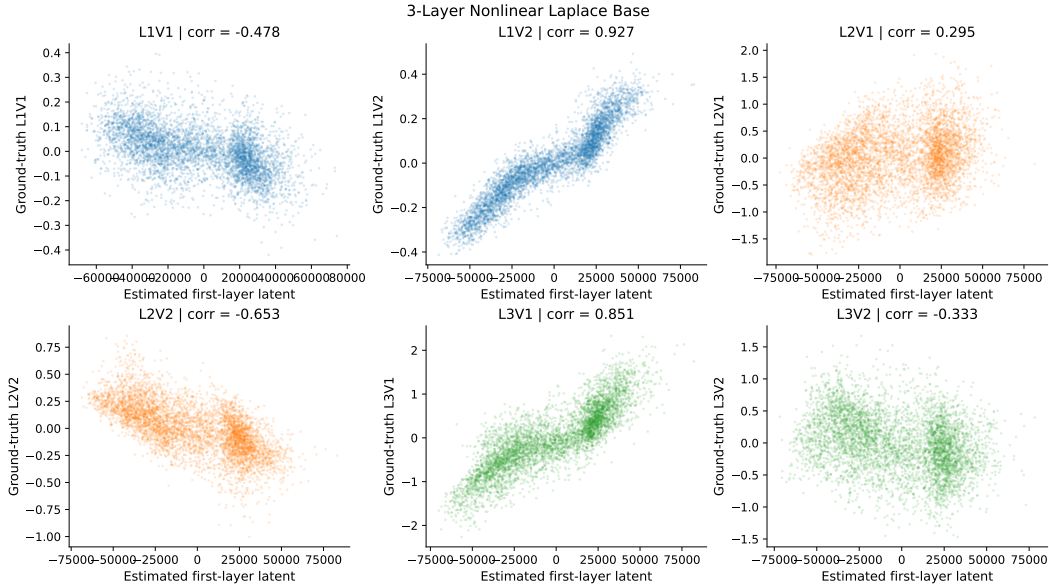


Figure 8: Three-layer synthetic experiment, full cross-layer comparison. Each panel compares the learned scalar first-layer representation with one ground-truth latent coordinate among the six coordinates spanning all three layers. The strongest alignment is attained on a first-layer coordinate, while several non-first-layer coordinates still exhibit sizable, though smaller, correlations.

layers to $L = 4$, providing sufficient depth to capture fundamental-to-specific concept gradients while remaining interpretable. For the VAR model order p , we evaluate $p \in \{10, 50, 100\}$: order 10 captures short-range token-level dependencies where hierarchical transitions are strongest (B-matrix weights $5\text{--}7\times$ larger than at $p = 100$ on AMPS), order 50 captures mid-range discourse structure, and order 100 serves as an upper bound confirming that the signal degrades at longer lags — consistent with hierarchical concept transitions in structured text being primarily a local phenomenon. For the inter-layer sparsity penalty $\lambda_{\text{sp}} \in \{10^{-4}, 10^{-5}\}$, both values produce consistent Gini concentration gradients on AMPS (L0 $\mu = 0.054$ vs. L2 $\mu \approx 0.039$ for both settings), confirming that hierarchy recovery is not sensitive to the precise sparsity level within this range. Unless otherwise stated, we report results at $p = 10$ and $\lambda_{\text{sp}} = 10^{-4}$, which yields the strongest B-matrix signal and clearest concentration gradient across all three datasets.

E.2.2 S-RQ2&3 Settings

E.3 Transition scenarios

All experiments use a shared data1 dataset generated from two active latent factors (z_1, z_2) observed through a random linear mixing matrix. The seven data2 transition scenarios vary which factors are retained, dropped, or newly introduced:

ID	Name	Active factors in data2	New dims
C1	No shift	z_1, z_2	0
C2	Full expand	z_1, z_2, z_3, z_4	2
C3	Drop all	z_3, z_4	2
C4*	Selective	z_1, z_3, z_4	2
C5*	Selective	z_2, z_3, z_4	2
C6	Keep one	z_1	0
C7	Keep one	z_2	0

Table 4: Seven transition scenarios. C4* and C5* (starred) are the hard selective cases requiring simultaneous reuse and expansion.

Evaluation metrics **Plasticity.** (target MCC): mean correlation coefficient between estimated and ground-truth latents on data2, maximized over permutations. Higher is better; scratch and fine-tune serve as upper-bound references.

Stability. (forgetting): difference between old-factor MCC before and after adaptation, $\Delta = \text{MCC}_{\text{old}}^{\text{before}} - \text{MCC}_{\text{old}}^{\text{after}}$. Negative values indicate backward transfer (adaptation improved old-factor recovery).

Gate accuracy (S-RQ3 only): fraction of binary gate decisions matching the ground-truth factor assignment, averaged over old and new modules.

Baselines

- **Scratch:** train a new encoder on data2 from random initialization; no knowledge transfer.
- **Fine-tune:** initialize from the data1 encoder and fine-tune all parameters on data2; no explicit stability mechanism.
- **Expansion only:** freeze the data1 encoder entirely and learn new modules for data2 factors; perfect stability by construction but cannot adapt reused modules.
- **MoRe w/o T :** full MoRe gating and sparsity losses, but the alignment matrix T is removed; tests the contribution of T to stability.
- **MoRe w/o $w_{\text{sp}}^{\text{old}}$:** MoRe without the sparsity penalty on old gates; tests whether old-module regularization is necessary for correct gate decisions.
- **MoRe w/o $w_{\text{sp}}^{\text{new}}$:** MoRe without the sparsity penalty on new gates; tests whether new-module regularization is necessary.
- **MoRe:** the full proposed method with uniform gate initialization, alignment T , and both sparsity penalties.

E.4 Hyperparameter selection

Hyperparameters are selected per scenario via random search over 8 configurations ($T = 50,000$ time steps, 3 seeds), evaluated by a composite score combining gate accuracy, target MCC, and forgetting. The selected ranges are: $w_{\text{sp}}^{\text{old}} \in \{0.005, 0.01, 0.05\}$, $w_{\text{sp}}^{\text{new}} \in \{0.001, 0.01, 0.05\}$, $w_{\text{align}} \in \{0.005, 0.02\}$, noise floor $\in \{0.3, 0.5\}$, $\tau_{\text{end}} \in \{0.2, 0.5\}$. All other hyperparameters are fixed: learning rate 5×10^{-3} , 2,000 training epochs, observation dimension 8, noise scale 0.1.

E.4.1 Extracted Low-to-High Layer Relations

F Extended Related Work

We review the literature from a relatively high-level perspective to show that a principled way for continual representation learning is missing, and the key can be a modular representation structure.

Supervised Continual Learning Continual learning (CL) is commonly framed as the problem of acquiring new capabilities without catastrophic forgetting. In supervised CL, many representative methods address this problem by constraining parameter updates, replaying information from previous tasks, or isolating parameters across tasks. Regularization and distillation methods—such as Elastic Weight Consolidation [11], Learning without Forgetting [13] and Memory Aware Synapses [1]—penalize changes that would harm previous tasks. Replay-based and exemplar-based methods, such as iCaRL [23], maintain or approximate past-task information while jointly learning classifiers and representations. Architecture-based methods instead allocate separate or partially separate computation to different tasks: Progressive Networks add task-specific columns with lateral transfer, PathNet learns task-specific paths through a shared module pool, and Expert Gate learns a gating mechanism that routes inputs to task-specialized experts [24, 5, 2]. A closely related line of work explicitly conditions computation on the task, such as Hard Attention to the Task [25] that learns nearly-binary attention masks that protect units used by previous tasks.

The Mixture-of-Experts (MoE) framework [26], in which a trainable gating network selects a sparse combination of feed-forward experts per example, provides a natural substrate for continual learning

Table 5: Representative cross-layer B-matrix links from the best setting (order $p = 10$, $\lambda_{sp} = 10^{-4}$, Pythia-1.4B). Each row shows a directed temporal dependency from a source-layer concept to a target-layer concept, annotated with the top-3 activating categories and the mean B-matrix weight (strength). AMPS links follow the curriculum direction (fundamental \rightarrow specific); arXiv links show abstract mathematics predicting applied domains.

Dataset	Block	Source concept (top categories)	Target concept (top categories)	Strength
<i>AMPS — curriculum hierarchy (arithmetic \rightarrow advanced linear algebra)</i>				
AMPS	L0 \rightarrow L2	L0_add, L0_simplify, L1_factor	L3_determinant, L2_matrix, L1_equation	0.078
AMPS	L0 \rightarrow L1	L1_equation, L1_factor, L0_simplify	L0_multiply, L1_equation, L2_matrix	0.063
AMPS	L1 \rightarrow L3	L1_factor, L0_simplify, L0_add	L3_determinant, L2_matrix, L0_multiply	0.045
<i>arXiv — abstract mathematics \rightarrow applied domains</i>				
arXiv	L1 \rightarrow L3	math.NT, math.LO, math.GM	math.CT, math.LO, physics.ins-det	0.011
arXiv	L1 \rightarrow L2	math.CT, cs.LO, cs.SE	math.GN, q-fin.CP, math.GM	0.010

Note: B-link strengths are 5–7 \times stronger on AMPS than arXiv (0.045–0.078 vs. 0.010–0.011), consistent with AMPS having cleaner sequential structure through its step-by-step curriculum format. arXiv strengths are weaker because domain category labels provide only a coarse proxy for abstraction level.

since new experts can be added without disturbing old ones. Recent analyses further formalize how expert specialization and routing reduce interference in continual task streams [12]. Lifelong-MoE [4] expands and freezes distribution-specialized experts and gating dimensions for continual language pre-training, while MoE-Adapters [39] attach task-specific adapter experts to a frozen vision-language backbone with a distribution-discriminative auto-selector. With large pre-trained models, parameter-efficient fine-tuning (PEFT) methods adapt only small task-specific components, such as adapters or low-rank updates, while freezing most backbone parameters [8, 10]. Building on this, recent CL methods constrain successive PEFT updates to interfere as little as possible with prior knowledge: O-LoRA [35] learns sequential LoRA updates in mutually orthogonal low-rank subspaces, and InfLoRA [15] reparameterizes pre-trained weights through an interference-eliminating subspace. Prompt-based continual learning extends the PEFT idea by learning small prompt memories or complementary prompts to manage task-specific and task-invariant knowledge without replay [37, 36, 27]. Despite their empirical strengths, these supervised CL methods predominantly treat forgetting as a parameter- or task-level phenomenon: experts, paths, prompts, and low-rank updates are defined and indexed by *tasks* rather than by the latent structure of the data, and consequently offer no principled way to separate fundamental, broadly shared knowledge from task-specific specializations. We argue that the underlying issue is fundamentally representational: tasks require representations that are simultaneously distinct (so updates do not interfere) and structured (so that what is shared is reused). Once such rich representations are obtained, a few labeled samples should suffice to specialize to any new task. MoRe takes this view explicitly, deriving its modular decomposition from identifiable factors of the data-generating process rather than from task labels.

Unsupervised Continual Learning A second line of work studies continual learning when labels or task identities are unavailable. CURL [22] introduced an unsupervised continual representation-learning setting in which the model infers tasks, dynamically expands to capture new concepts, and uses rehearsal to reduce forgetting. In the SSL setting, Hu et al. [9] evaluate sequential self-supervised pre-training on streaming ImageNet and DomainNet, using downstream transfer tasks to measure whether learned representations both adapt and avoid forgetting; they find that simple replay or parameter regularization can make sequential SSL close to joint pre-training in many settings,

while severe distribution shifts remain challenging. LUMP [18] further observes that unsupervised representations forget less than supervised ones and proposes mixup interpolation between current and replayed instances. CaSSLe [6] converts SSL objectives into temporal distillation by mapping current representations to past ones, improving continual self-supervised visual representation learning across several SSL losses. PFR [7] and Kaizen [30] extend this predictor-based framework to mitigate plasticity loss and to jointly train feature extractors and classifiers. Most closely related to our motivation, Branch-Tuning [16] analyzes stability and plasticity using centered kernel alignment and proposes branch expansion/compression, fixing existing components while adding trainable convolutional branches for new data and then reparameterizing them back into the network. These methods clarify that continual SSL should be evaluated at the representation level, rather than only by immediate training losses. However, their adaptation mechanisms still operate by replay, distillation, regularization, or branch modification. MoRe instead asks what representation structure makes such selective adaptation principled: we posit and identify a hierarchical modular representation, enabling adaptation to be localized to the modules whose latent factors have changed.

Modular Network for Continual Learning Modularity is a long-standing strategy for managing the stability–plasticity trade-off [34]. Recent work has unified adapters, MoE layers, sparse subnetworks, and prompt mixtures under a common modular framework that highlights CL as a canonical setting where modularity should help [20]. Progressive networks add a new column for each task and connect it laterally to previous columns [24]; PathNet evolves task-specific paths through a fixed pool of modules [5]; Expert Gate learns a network of experts and uses gating autoencoders to select the relevant expert at test time [2]; hard-attention and pruning approaches learn task-specific masks or reuse freed parameters to protect old tasks [25, 19]; and MNTDP [33] maintains a library of modules and decides per task which to reuse and which to add via a data-driven prior. Modular adapter approaches extend the same idea to parameter-efficient adaptation of pretrained transformers [21], and sparse mixture-of-experts architectures similarly route inputs to subsets of capacity [26]. These approaches instantiate *architectural* modularity: modules are usually experts, subnetworks, masks, prompts, or adapters that are introduced or selected according to tasks, heuristics, or learned gates. MoRe is complementary but different: it learns *representational* modularity, where modules correspond to latent components organized by a hierarchy in the data-generating process, with identifiability guarantees obtained from time-delayed cross-layer dependencies. The decomposition is therefore not merely a convenient allocation of parameters but a principled reflection of structure in the data, providing a basis for preserving fundamental knowledge while updating more specific components without requiring a task oracle.